

ABSTRACT

LEHMAN, TED EUGENE. High Aspect Ratio Microhole Drilling with Rapidly Repeated Pulses. (Under the direction of Juei-Feng Tu.)

The necessity for micro holes spans across a wide range of industrial applications with nearly endless boundaries. From electronics and X-Ray apertures to micro fluidics and heat transfer phenomenon, the advancement of precision ablation will undoubtedly be of benefit.

Currently, three major techniques are employed in the fabrication of micro-holes:

Conventional drilling methods, electrical discharge machining (EDM), and laser drilling. The flexibility to drill a wide range of materials with a single device in combination with high consistency and accuracy lead many applications to the necessity of laser drilling. Major drawbacks of laser ablation are low material removal rates and heat affected zones around the holes. Much research has been performed in the pico- and femtosecond paradigm with less insight into longer pulse durations. Investigation was conducted into four variables affecting microsecond pulses on the material removal of steel: pulse length, high power density spikes, pulsing frequency, as well as group multiple pulsing. The optimal pulse length of 3 μs created unblocked holes with aspect ratios of 6 and depths of 196 μm . Multiple pulsing increased the aspect ratio to 10, deepening the cavity to 236 μm . Optimum depth occurred with the maximum number of pulses tested, 10; producing an aspect ratio of 12 and a depth of 295 μm . A major drawback produced by 10 pulses was the signs of hole blockage. A process anatomy of hole creation explains causes of the blockage. The second variable, high power density spike exhibited by the laser increased hole depth 5% over instances lacking this spike. Major improvements in depth were demonstrated as the pulsing frequency was increased to a laser capable maximum of 48.7 kHz. Holes created under this condition experienced major blockage near the exit. Group multiple pulsing deepened the hole to 438 μm with three sets of ten pulses at 48.7 kHz. Holes exhibited extreme blockage throughout their depths.

Efficient, High Aspect Ratio Microhole Drilling
with Rapidly Repeated Pulses

by
Ted Eugene Lehman

A thesis submitted to the Graduate Faculty of
North Carolina State University
in partial fulfillment of the
requirements for the Degree of
Master of Science

Mechanical Engineering

Raleigh, North Carolina

2009

APPROVED BY:

Dr. Tarek Echehki

Dr. Fuh-Gwo Yuan

Dr. Juei-Feng Tu
Chair of Advisory Committee

BIOGRAPHY

Ted Eugene Lehman was born April 29th, 1985 in Wiesbaden, Germany. Before college, he spent years in both the American and German school systems. After spending his High School at an American High School in Germany, he decided on American Universities to begin his Engineering schooling. He transferred to The North Carolina State University from Tulane University in New Orleans, Louisiana after his freshman year. In 2008, he graduated with his Bachelor of Science in Mechanical Engineering.

ACKNOWLEDGEMENTS

The major accomplishment of this research and my degree would not have been possible if it were not for the help other's volunteering in my aid. My advisor, Dr. Tu significantly impacted not only my research, but my life. Dr. Tu broadened my view of the world and provided new structure in the way I view challenges. His time and commitment to education and learning is a profound model I will always admire. I would also like to thank Dr. Echecki and Dr. Yuan for serving on my committee board. Additionally, the time and insight Dr. Paleocrassas donated guided me through the journey. Nilesh Rajule, my lab partner, not only acted as a sounding board but also was a friend in the many hours spent in the lab.

In a less direct manner, yet just as vital, I must thank my family for the support and the environment they created to shape me through the years.

TABLE OF CONTENTS

List of Figures	vi
1 Introduction	1
1.1 Significance of the Problem	1
1.2 Motivation	2
2 Background Information	3
2.1 Macroscopic view of Laser Ablation	3
2.2 Microscopic view of Laser Ablation	9
3 Literature Review.....	13
3.1 Pulse length effects on hole quality and material removal rates.....	13
3.2 Insight into the multiple pulse paradigm	16
4 Specific Research Objective	17
5 Research Approaches	18
6 Experimental Apparatus	20
7 Experimental Procedures.....	32
7.1 InGaAs Photodiode Calibration.....	32
7.2 Focus Test.....	33
7.3 Single Pulse Test	33
7.4 Multiple Pulse Test	34
7.5 Plasma Measurement.....	34
7.6 Sample Grinding/Polishing	35
8 Results and discussions.....	36
8.1 Single Pulse Results	36
8.2 Process Anatomy of Single Pulse	40
8.3 Triple Pulse Results	42
8.4 Process Anatomy of Multiple Pulses.....	46
8.5 Ten Pulse Results	48

8.6 Effects of High Initial Power Density.....	52
8.7 Effects of Pulse Frequency.....	56
8.8 Group Multiple Pulse Drilling.....	62
8.9 Through Drilling.....	65
9 Summary.....	69
References.....	71
APPENDIX.....	75
Appendix I.....	76

LIST OF FIGURES

Figure 2.1-1: Energy balance	3
Figure 2.1-2 : Reflectivity of Platinum ⁽²⁾	5
Figure 2.1-3 : Variation of Reflectivity due to Wavelength ⁽¹⁾	6
Figure 2.1-4 : Variation of Reflectivity due to Temperature ⁽³⁾	7
Figure 2.2-1: The electric and magnetic field vectors of electromagnetic radiation. ⁽⁵⁾	9
Figure 2.2-2: Scattering Mechanisms of free electrons in a metal ⁽⁶⁾	10
Figure 2.2-3: Schematic of UV Laser Ablation Events ⁽⁹⁾	11
Figure 3.2-1: 300 W Ytterbium, single-mode fiber laser power unit	20
Figure 3.2-2 : Optical isolator connection to collimator, used to divert away reflected laser light into a beam dump	21
Figure 3.2-3: XY Linear motors with attached work plate fixture	22
Figure 3.2-4: Galil X-Y axes motion controllers	22
Figure 3.2-5: dSPACE 4.0 data acquisition system	23
Figure 3.2-6 : Beam expander and laser head setup	24
Figure 3.2-7: X,Y,Z micrometer linear stages	25
Figure 3.2-8: Circuit Control Box Interface	27
Figure 3.2-9: Circuit Board for Multiple Pulse Laser Control: Digital and Analog	27
Figure 3.2-10: Tektronix 3012B oscilloscope	28
Figure 3.2-11: Zeiss Inverted Microscope	29
Figure 3.2-12: Saphir 520 Grinder/Polisher	30
Figure 3.2-13: Hamamatsu Si S1336-B18BQ photodiode Spectral Response	31
Figure 3.2-14: Hamamatsu InGaAs G8370 Photodiode Spectral Response	31
Figure 8.1-1: Input Pulse and associated Pulse Waveform for Single Pulse.....	37
Figure 8.1-2: Hole Profiles Produced by 1 Pulse	38
Figure 8.1-3: Plasma ejection of a Single Pulse on Steel.....	39
Figure 8.2-1: Process Anatomy of Single Pulse Ablation.....	40
Figure 8.3-1: Input Signal and Laser Pulse of Multiple Pulses.....	42
Figure 8.3-2: Pulse Waveform and Plasma Intensities of 3 Pulse Digital Circuit	43
Figure 8.3-3: Pulse Waveform and Plasma Intensities of 3 Pulse Analog Circuit	44
Figure 8.3-4: Hole Profiles Produced by 3 Pulses.....	45
Figure 8.4-1: Process Anatomy of Multiple Pulse Ablation.....	46
Figure 8.5-1: Pulse Waveform and Plasma Intensities of 10 Pulse Digital Circuit	48
Figure 8.5-2: Pulse Waveform and Plasma Intensities of 10 Pulse Analog Circuit	49
Figure 8.5-3: Hole Profiles Produced by 10 Pulses.....	50
Figure 8.5-4: Relationship between Hole Depth and number of Pulses	51

Figure 8.6-1: Pulse Waveform and Plasma Intensities of 10 Pulse Digital Circuit at 16.1 kHz	52
Figure 8.6-2: Pulse Waveform and Plasma Intensities of 10 Pulse Analog Circuit at 16.1 kHz	53
Figure 8.6-3: Hole Profiles from 10 pulses at 16.1 kHz	54
Figure 8.6-4: Hole Depth Comparison with variations in Power Density of 10 Pulses at 16.1 kHz	55
Figure 8.7-1: Pulse Waveform and Plasma Intensities of 10 Pulses at 31.5 kHz	57
Figure 8.7-2: Pulse Waveform and Plasma Intensities of 10 Pulses at 42.8 kHz	58
Figure 8.7-3: Pulse Waveform and Plasma Intensities of 10 Pulses at 48.7 kHz	59
Figure 8.7-4: Hole Profiles Created at Different Pulsing Frequencies	60
Figure 8.7-5: Hole Depth in Relation to Pulsing Frequency	61
Figure 8.8-1: Hole Profiles from Group Single Pulse Drilling.....	62
Figure 8.8-2: Hole Profiles from Group 10 Pulse Drilling	64
Figure 8.9-1: Time required for a through hole of 800 microns at 20 kHz.....	65
Figure 8.9-2: Time required for a through hole of 800 microns at 13 kHz.....	65
Figure 8.9-3: Hole Profiles of 800 Micrometer Through Holes	66
Figure 8.9-4: Time required for a through hole of 1.1 mm at 13 kHz	67
Figure 8.9-5: Time required for a through hole of 1.1 mm at 20 kHz	67
Figure 8.9-3: Hole Profiles of 800 Micrometer Through Holes	68

1 Introduction

1.1 *Significance of the Problem*

The necessity for micro holes spans across a wide range of industrial applications with nearly endless boundaries. From electronics and X-Ray apertures to micro fluidics and heat transfer phenomenon, the advancement of precision ablation will undoubtedly be of benefit. A novel use of micro holes is the creation of flexible circuits in which lasers ablate organic material from gold contact pads. The precision required is attributed to the need to remove material without damaging surrounding areas. Applications of such technology can be seen wherever electronics are present. Most notably, flexible circuits hope to advance the sciences of printers, automotive industries, as well as medical electronics. Medical devices lend themselves perfectly to the idea of micro-hole drilling; Catheters, irrigation needles, and precise orifices for oxygen regulators are some of the direct applications. Trends towards fabricating pinholes, air slits, collimators, and spatial filters for non-destructive, non-contact illumination devices are requiring high dimensional tolerance, repeatability, and resolution. Along with the medical device industry, pharmaceuticals and beverage packaging companies stand to benefit from precision holes. Improved leak test equipment is pushing the limits of calibrated leak holes. Smaller, more precise flow orifices are of high demand for accuracy and repeatability of flow calculations. Such innovations will immediately be used in foil packages in the medical device industry as well as blister packs and plastic ampoules for pharmaceutical reasons. Other applications currently employed are aerospace combustor liners, fuel injectors, filters, turbine blades, and air bearings.

The above mentioned applications are not all inclusive as unique uses are currently under investigation. The number of uses will continue to increase as advanced metals, glass and plastics are researched and implemented in industry.

Currently, three major techniques are employed in the fabrication of micro-holes: Conventional drilling methods, electrical discharge machining (EDM), and laser drilling. Conventional drilling methods are limited in scope. This method involves a miniature milling machine with a drilling bit having a diameter of the hole desired. Holes produced by this method must be greater than 25 microns in diameter. Hole characteristics are good as clean, circular holes are created. EDM is a more viable industrial application. Through a series of rapid current discharges between the electrode and the work piece, EDM is able to remove material in any shape. Micro-hole drilling has been accomplished with hole diameters as small as 70 micrometers and aspect ratios between 300 and 400. Other advantages of EDM drilling include burr less holes at both the entry and exit edges as well as the ability to drill work pieces already in the hardened condition. Laser drilling, also known as laser ablation, is widely used to create high quality holes in a range of materials. Hole diameters reach a minimum of 5 microns with aspect ratios of ~30.

1.2 Motivation

Laser drilling has many advantages to conventional drilling techniques. First, laser drilling, being an optical energy process, is non-contact. The flexibility to drill a wide range of materials with a single device in combination with high consistency and accuracy lead many applications to the necessity of laser drilling. Currently, major drawbacks include tapered holes, heat affected zones, limited depth and diameter, and recast layers within the hole. Because of these drawbacks laser drilling has yet to reach its full industrial potential. Therefore, research into higher aspect ratio holes will open doors currently unattainable to the laser drilling paradigm.

2 Background Information

2.1 Macroscopic view of Laser Ablation

Laser material processing is a complicated interaction between the beam and the processing material. Any process, whether it is welding, cutting, drilling, alloying and so forth, relies on the absorption of the emitted energy. Many characteristics of the beam itself affect the ability to perform the required tasks. Beam quality, output power, processing speed, and beam shape are just a few considerations to be taken into account throughout laser fabrication. More fundamentally, energy absorption can be broken down into three main avenues as illustrated in Figure 2.1-1.

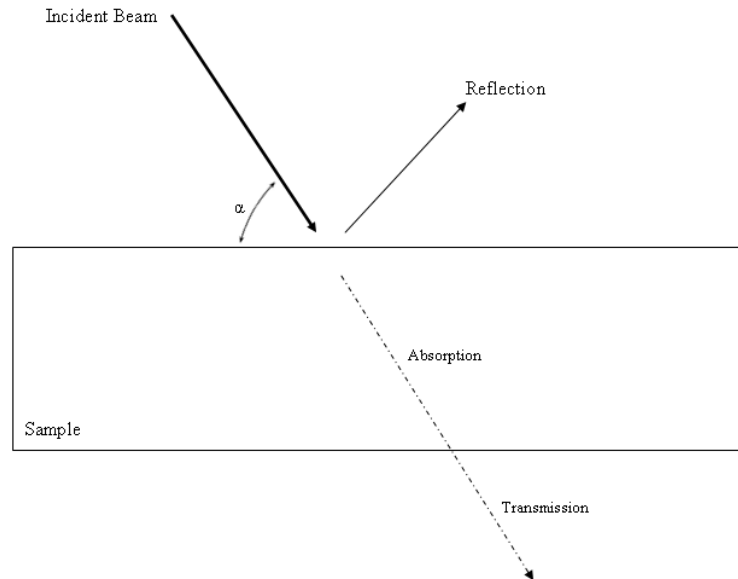


Figure 2.1-1: Energy balance

Relying on Figure 2.1-1 it is possible to follow all paths the laser energy may take. The irradiation from the laser hits the sample at an angle of incidence, alpha. From this

irradiation, some energy will be reflected from the surface of the material while the rest is absorbed. Depending on the material, whether opaque or not, energy may be allowed to be transmitted completely through the sample. Thus, wasted energy can be attributed to both reflection and transmission. However, most metals are opaque and transmission does not occur. From this energy balance an analytical comparison of the different energy paths is possible. The terms reflectivity (ρ), absorptivity (α), and transmissivity (τ) are introduced to aid in energy balance formulation and are defined as:

$$\begin{aligned}\rho &= \frac{\text{reflected radiation}}{\text{total radiation}} \\ \alpha &= \frac{\text{absorbed radiation}}{\text{total radiation}} \\ \tau &= \frac{\text{transmitted radiation}}{\text{total radiation}}\end{aligned}\tag{2-1}$$

As defined, all irradiative properties are a fraction of total radiation. Understanding that all radiation must be reflected, absorbed, or transmitted, it follows that

$$\mathbf{1 = \rho + \alpha + \tau}\tag{2-2}$$

Including the notion of metal, particularly steel, as being opaque, no radiation will be transmitted, $\tau=0$:

$$\mathbf{1 = \rho + \alpha}\tag{2-3}$$

Concluding from equation 2-3, minimizing reflected radiation at the surface will enhance the absorption into the metal.⁽¹⁾

Reflection

As shown above, a percentage of irradiation will reflect from the surface of the material and be “wasted” as no absorption occurs. Because of this, reflection should be minimized in order for the greatest use of radiation. Reflectivity is affected by three parameters; angle of incidence, wavelength, and temperature.

Figure 2.1-2 although calculated only for platinum, shows the trends changing the angle of incidence has on reflectivity.⁽²⁾

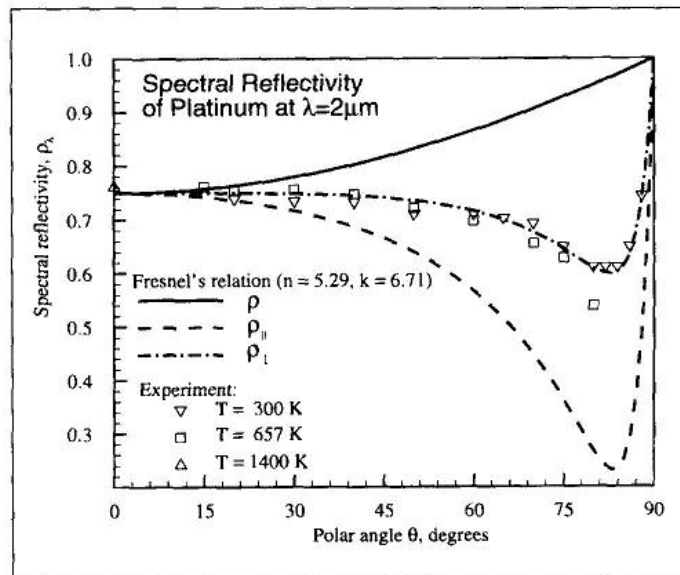


Figure 2.1-2 : Reflectivity of Platinum⁽²⁾

From Figure 2.1-2 it is seen refraction occurs least at normal incidence and peaks near perfect reflection as parallel incidence is approached. Such trends are typical among metals subjected to infrared radiation. ⁽²⁾

Irradiative wavelength also effects the reflective interactions between radiation and material absorption. Analyzing Figure 2.1-3 allows for the approximation of reflectivity of steel in light of different laser types.

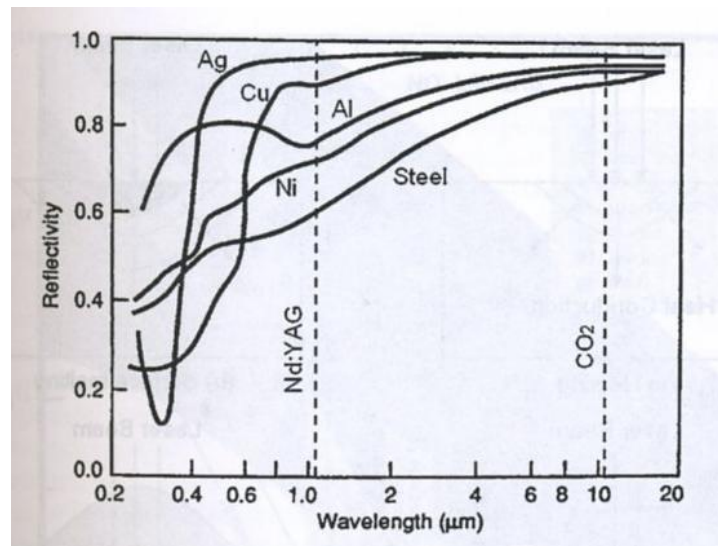


Figure 2.1-3 : Variation of Reflectivity due to Wavelength ⁽¹⁾

The fiber laser in use will produce a reflectivity near .6 when induced on steel. The same sample would experience a reflectivity of nearly .9 using a CO₂ laser. This implies reflectivity, in general, decreases with decreasing wavelength.

Temperature effects are less general and require more insight into its effects.

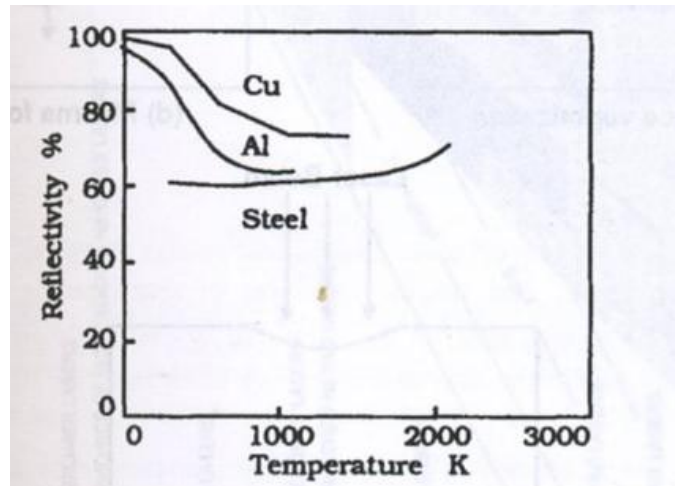


Figure 2.1-4 : Variation of Reflectivity due to Temperature ⁽³⁾

Figure 2.1-4 depicts copper's, aluminum's, and steel's reflectivities against temperature. Copper and aluminum, both having high reflectivities at low temperatures, experience drastic drops in reflectivity as temperature is increased. However, the reflectivity of steel increases slightly over the same temperature rise. As a guideline, materials with high reflectivity at low temperatures have an inversely related reflectivity to temperature while materials initially experiencing low reflectivity will increase as temperature increases. ⁽⁴⁾

Absorption

Absorption is a material based property heavily influenced by the electron configuration of the sample. ⁽⁴⁾ Across all materials absorption is a function of radiation wavelength and temperature.

As mentioned, most metals can be considered opaque, and thus no radiation is transmitted through the sample. This assumption is based on the transmissivity of material:

$$\tau = e^{-\kappa L}$$

(2-4)

Where κ is the material's absorption coefficient and L describes the layer thickness. Materials with κL values of 3 are considered optically opaque. Metals, having κ on the order of 10, are often considered opaque at thickness of merely 100 nm. This assumption allows for the neglect of the τ term in equation 2-2 giving us the simplified equation 2-3.

Equation 2-3 directly couples absorptivity to reflectivity. Therefore an increase in one will decrease the other. Applying this logic to already mentioned graphs, trends can easily be drawn between absorptivity and wavelength as well as temperature.

First, the angle of incidence will undoubtedly change the absorptive properties of the setup. As shown in Figure 2.1-3, reflectivity is minimized at normal incidence. This, in combination with equation 2-3, implies absorption will maximize at normal incidence.

Decreases in wavelength, in accordance with Figure 2.1-3, will decrease reflectivity. This is beneficial to material processing as absorption into the material will increase.

Finally, temperature effects must be taken into consideration. This must be done on a case by case basis as materials will be affected drastically differently. Reflectivity of steel is not affected greatly by temperature, Figure 2.1-4, remaining near .6. If other materials such as copper or aluminum are to be used, the determination of optimal temperature may improve fabrication.

2.2 Microscopic view of Laser Ablation

As shown above, radiation can be affected by a material in three ways: reflection, absorption, and transmission. Experimental focus, however, is not merely on the laser energy, but directly involves the interaction between the mentioned energy and a sample material.

With respect to the material, reflected and transmitted energies play no integral role in material processing as it is “wasted” to the surroundings. The absorbed energy directly interacts with the material on an atomic level, and thereby generates the phase transitions desired for processing. Absorption of the radiation as it passes through the medium acts in close accordance to Beer Lambert’s law:

$$I = I_0 e^{-\beta z}$$

2-5

B is the absorption coefficient, relying on the medium as well as the radiation wavelength and intensity. I_0 represents the light intensity and z is the depth of penetration. Laser radiation, being electromagnetic, can be modeled by both an electric vector field and a magnetic vector field as shown in Figure 2.2-1.

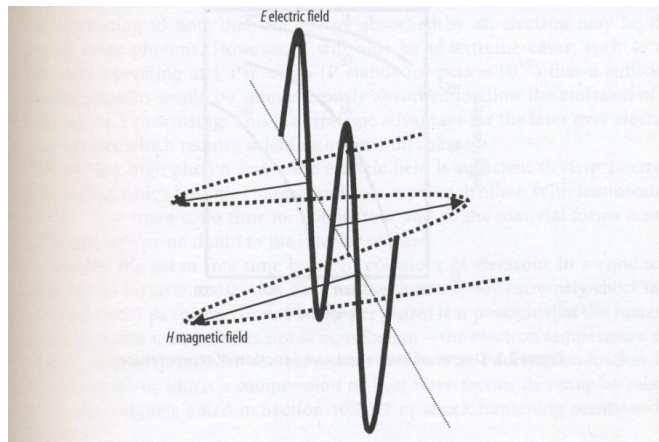


Figure 2.2-1: The electric and magnetic field vectors of electromagnetic radiation. ⁽⁵⁾

Photons from the electric field produce a force, too weak to affect the atomic nuclei, which vibrates the electrons, whether free (in metals) or bonded, within a material. As the photons

are absorbed in a process known as the “inverse bremsstrahlung effect” their interaction with the surrounding material will be conducted in one of two ways: The electron will either re-radiate in all directions, or it will be confined by the surrounding lattice phonons. This vibration will continue into the structure, passed from one electron to the next, producing heat. ⁽⁵⁾

More specifically, heat is conducted through the material using four possible avenues. Electron-electron scattering, electron-lattice scattering, boundary scattering, and defect scattering, as shown in Figure 2.2-2, are all methods heat is transferred. ⁽⁶⁾

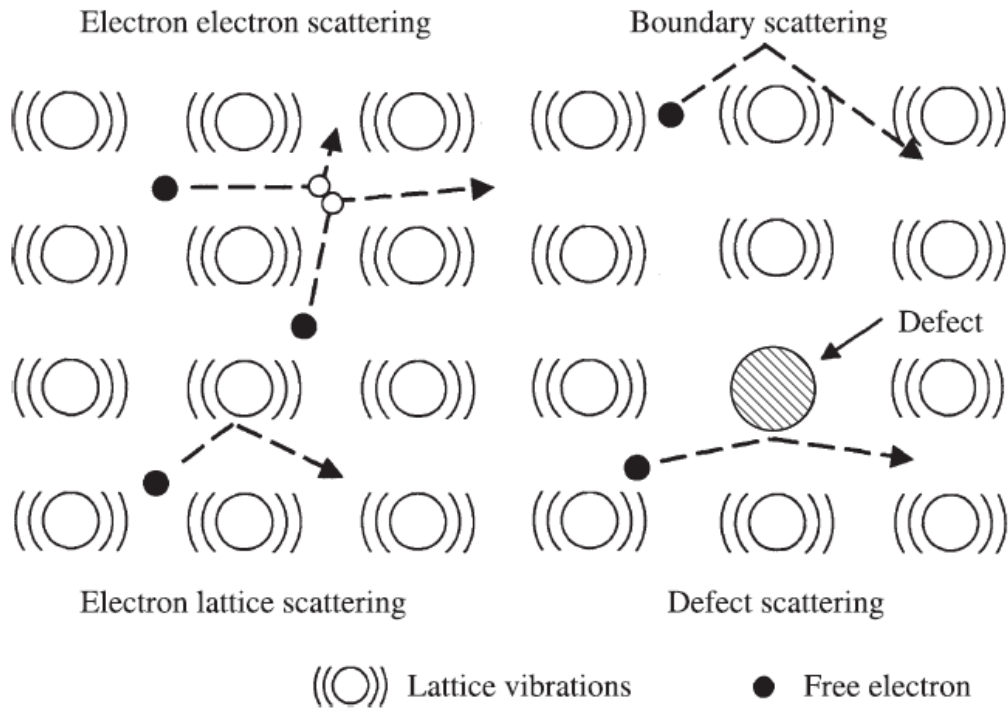


Figure 2.2-2: Scattering Mechanisms of free electrons in a metal ⁽⁶⁾

In the case of metals, this vibration and heat transfer weakens the molecular bonds creating a softer, and eventually molten, phase. Radiating the material further excites the outermost

electrons inducing evaporation and eventually plasma. The formation of plasma is expected at sufficient power densities in laser ablation.^[(7)-(8)] Figure 2.2-3 visualizes the heat transfer occurring throughout thermal ablation. This process, in which a sample is heated through the phases of molten, vapor, and plasma, is known as thermal ablation.

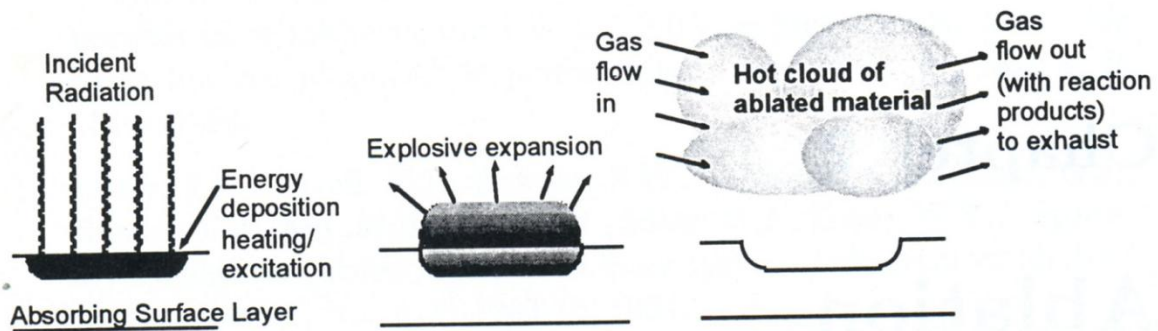


Figure 2.2-3: Schematic of UV Laser Ablation Events⁽⁹⁾

The thermal ablation process is a relatively long process producing holes with heat affected zones around the radiated area. This thermally affected zone can be minimized by inducing sufficiently high power densities in a short amount of time. As the electron is energized by a photon, it requires a finite length of time to begin vibrating, and thus transfer heat. Electrons absorb photons on the order of 10^{-15} seconds. Vibration of the electron is negligible until $\sim 10^{-12}$ seconds. This time required for vibration to begin is known as the relaxation period.⁽¹⁰⁾ By inducing a sufficiently high power density into a material within the relaxation period, the material will not have time to transfer heat to its surrounding. In such a case, an electron, being bombarded with an overwhelming number of photons, may absorb two or more photons. This highly energized electron is then stripped from its energy level, leaving a weakened material behind. The ejection also leaves a pressure difference at the surface where the weakened material sits. This newly induced pressure gradient forces the weakened material away from the sample, leaving a void. This is done so rapidly, $t < 10^{-12}$ seconds, that

the surrounding has seen no transfer of heat from the initial radiation. This process, leaving no sign of thermal damage, is known as “cold” ablation. Pulse durations on the femtosecond timescale qualify under this time constraint. Picosecond pulses, although not always shorter than the relaxation time, are on the same order, and therefore are considered to be cold ablation processing.

Research presented is a thermal ablation process on the order of microseconds. Laser energy will be coupled with elevated vapor and plasma temperatures to increase the efficiency of energy absorption. The increased energy input by both vapor absorption and increased pulse lengths will be investigated in material removal rates

3 Literature Review

The topic of laser ablation has been the focus of routine studies. The idea of light as a source of energy has been around for thousands of years. 303 B.C. it was recorded by Greece Lactinius, that a glass sphere filled with water is "sufficiently good to light a fire".⁽¹¹⁾ Laser ablation, inherently requiring advances in technology, did not appear until 1962 when F. Breech and L. Cross offered their findings at the International Conference on Spectroscopy at the University of Maryland. Their research was carried by ablating material with a ruby-red laser. The emitted light was then collected and spectrally dispersed birthing the age of laser ablation.⁽¹²⁾ One year later, J.J. Murray covered fundamental elements of laser ablation.⁽¹³⁾ Still today, the elements he investigates are researched with greater sophistication and detail.⁽¹⁴⁾

Since these preliminary findings, years of studies have investigated a wide range of variables relating to laser ablation. With regards to research pertaining to the discussion at hand, particular interest is paid to the research in pulse length, and multiple pulse experiments. More specifically, a comprehensive comparison of the effects such variables have on hole quality and material removal rate will aid in the hypothesis of medium length multiple hole drilling.

3.1 Pulse length effects on hole quality and material removal rates

Short and ultra-short pulses are quantified with respect to the relaxation time of the electrons within the ablated sample. Thermalization of the electrons requires a mere 100 fs.^[(15)(16)] Thermal effects of the surrounding lattice are witnessed near 100 ps.⁽¹⁷⁾ Pulses occurring on this timescale and shorter are considered short and ultra-short, respectively.

With ever increasingly strict quality requirements, including high accuracy, and melt-free processing ⁽¹⁷⁾, hole quality quantification must be outlined and applied to quantify the quality of created holes. Measurements of hole quality is objectively set forth by Yilbas. The comprehensive, and widely accepted, model attributes two thirds of hole quality to heat affected phenomena. ⁽¹⁸⁾ Following this model, it can be hypothesized energy radiation occurring quicker than the 100 ps relaxation time, would produce the highest degree of hole quality, as time does not allow for heat effects to occur. The phenomenon created by femtosecond laser ablation has been documented thoroughly across the years. ^[(19)(20)(21)(22)(23)(24)] These studies repeatedly, under different fluences, laser types, and sample materials, create holes showing minimal to no signs of thermal damage. Holes witnessed are of superior quality in terms of surface debris, barreling, re-solidification of material and inlet cone; further supporting the notion of minimal heat effects. Similar experimentation has been conducted in the regime of picoseconds ablation. ^[(25)-(26)] Consistent findings throughout material type, time length (in the picosecond regime), laser characteristics, show definite signs of thermal damage of the ablated holes. Proof of thermal effects is witnessed through poor wall quality, surface debris, and even signs of metal re-solidification. When femtosecond ablation is directly compared to picoseconds ablation under similar circumstances ^[(17)(27)(28)(29)], a more direct conclusion can be drawn. Each of these studies compares femto vs. pico second laser pulses on similar sample materials, within the same environment, under similar circumstances. Without fail, the femtosecond pulses produced holes of higher quality.

B.N. Chichkov presents a yet more detailed and applicable account of femtosecond, picoseconds, and nanosecond laser ablation processes. ⁽²⁷⁾ Chichkov's findings of hole quality and drilling rates compare all three radiation regimes on identical samples. Experiments were conducted on steel samples, among others, with pulse lengths of 200 fs, 80 ps, and 3.3 ns. Each length is specifically chosen to represent an increased pulse lengths in the ultrashort paradigm, allowing conclusions to be made concerning increased pulse length.

Again, it was shown femtosecond pulses create the cleanest holes, showing minimal signs of thermal damage. Nanosecond findings show walls raised above the surface of the material, evidence of material removal by both liquid and vapor phases.

Zhu reports similar findings using femtosecond, picoseconds, and nanosecond pulses on aluminum.⁽³⁰⁾ Experiments were used by irradiating aluminum samples for durations of 60 fs, 50 ps, and 10 ns. Consistent with past findings, femtosecond holes were of best quality while the nanosecond pulses had moderate quality. Zhu's findings, shed light on drilling rate affects from each method. Through atomic force microscopy, it was determined hole depths were 1.1-, 0.6-, and 1.6 μm for femtosecond, picoseconds, and nanosecond samples, respectively. Such findings show evidence nanosecond ablation is a viable option given necessity for high material removal rates with slightly relaxed requirements on hole quality.

Both the above mentioned papers clearly show increased ablation times have two effects on hole creation. First, the removal rate is increased. Second, the hole quality experiences degradation. For holes requiring high removal rates yet not as perfect hole quality, longer pulses become ideal.

The lack of available laser sources has led to a lack of literature on microsecond pulse ablation.⁽³¹⁾ Pulse durations were created using a Q-switched Nd:YAG laser with an adjustable length resonator with an optical fiber of various lengths. Pulse durations of .15, 1.1, and 4.5 μs were used in order to show microsecond laser pulses could achieve a compromise between ablation rate and hole quality. Aluminum, stainless steel, alumina ceramic, and graphite were all subjected to a 375 μm diameter spot. The repetition rates were documented between 1- and 10 Hz. Hole depths in aluminum were 30 $\mu\text{m}/\text{pulse}$, 10 $\mu\text{m}/\text{pulse}$, and 1 $\mu\text{m}/\text{pulse}$ for 4.5 μs , 1.1 μs , and .15 μs pulses respectively. Stainless steel experienced 11 $\mu\text{m}/\text{pulse}$ for 4.5 μs pulses. This rate dropped to 6 $\mu\text{m}/\text{pulse}$ and 0.5 $\mu\text{m}/\text{pulse}$ for the 1.1 μs and 0.15 μs pulses respectively. Ceramics experienced even smaller rates but saw excellent hole quality.

3.2 Insight into the multiple pulse paradigm

To achieve maximum depth, logic leads to the notion of simply presenting two or more pulses onto a sample. Each successive pulse introduces more energy to the sample, and therefore ablates the material further. Recent research done by a number of groups has given great insight into the mechanisms of multiple pulse ablation.

In 2007, the department of physics at the University of “Politehnica” of Bucharest, Romania, presented a thorough theoretical model of multiple-nanosecond laser pulse irradiation.⁽³²⁾ In order to model the intricate process of ablation, a new photo-thermal model was presented in which complex phenomena of the process are accounted for as supplements to the classical heat equation. Melt ejection and evaporation are the determining factors for ablation due to recoil pressure created by the expanding plasma plume. Absorptions due to the plasma plume, molten and vaporized material were all taken into account during simulation. In addition to ablated material, the decrease in laser intensity is also accounted for due to increases in hole depth, diameter, and laser reflection within the hole. Simulation shows multiple pulses will increase the hole diameter, the peak intensity of the beam at the sample surface decays, and that the material removal rate decreases exponentially as the number of pulses increases.

Definite benefits of multiple pulse ablation are shown through findings conducted by C. Lehane, in which the delay time between shots of an Nd:YAG laser were altered.⁽³³⁾ The experiment conducted introduced an initial high intensity shot followed by a secondary shot of lower intensity. By altering the period between shots, Lehane was able to reduce the number of through hole pulses of a 1/16” stainless steel sample from 54 to 2 pulses. This work improved the process efficiency 27 times by the introduction of a secondary, much weaker pulse onto the sample.

Recent advance in multiple pulse drilling have been demonstrated by the photonics Division of General Atomics.⁽³⁴⁾ The novel technique presented allows pulses to be shot in quick

succession, with delays between 30- and 150 ns. Pulse lengths were 4 ns, with 1.2 mJ per pulse. Findings increased depth per pulse from 0.7- to 1.6 μm , for one pulse and one superpulse respectively. A 914 μm thick 304 stainless steel sample required 10,000 shots to penetrate. Major advances were in hole quality as the extremely quick succession of shots creates holes of “femtosecond quality”.

Application of the above mentioned technique was applied to picosecond pulsing by the Penn State Electro-Optics Center. ⁽³⁵⁾ Again, pulses were spaced between 20ns and 200 ns apart with pulse durations of 10ps. Improvements in hole quality were witnessed with an increase in material removal by a factor of 2.

Microdrilling in the μs paradigm has received minimal attention in the literature. Distinct advantages of very high material removal rates inspires further investigation. Focus will be on μs laser drilling with the addition of multiple pulsing to extend microhole drilling to very high aspect ratios with large material removal rates. The research to be conducted will differ from already discovered findings two fold. First, the laser input is on the order of microsecond, not pico- or femtoseconds. The goal is therefore not to create high temperature plasma, but to remove molten metal by inputting more energy per pulse using the longer pulses. Improvements in material removal per pulse are sought. Secondly, group pulsing schemes will be investigated to produce deep holes, rather than through holes, that are clear of molten material.

4 Specific Research Objective

The research objective of this thesis is to test the following hypothesis:

Efficient material removal in high-aspect micro-hole drilling can be accomplished if subsequent laser pulses can be used to energize molten or vapor materials providing sufficient kinetic energy to escape the cavity.

5 Research Approaches

In order to successfully complete the above research objective, the following approaches were developed.

First, determination of the optimal single pulse length was conducted. This was done by fitting an InGaAs photodiode with an operating wavelength range near 1075 nm to the unfocused laser. A calibration curve of the diode was created using the known steady state power output of 300W . The peak power output of the laser was then measured using the calibrated photodiode. Next, ablation efficiency using 1 μ s, 2 μ s, 3 μ s, 5 μ s, and 10 μ s pulses was investigated. Aspects of the hole taken into account were the hole's aspect-ratio, the plasma ejection during drilling, and the overall hole integrity.

For multiple pulse drilling, the next step dictated to create and verify controls for multiple pulsing. Steps to complete this were to create logic controls allowing for the variation of the initial pulse length, the subsequent pulse lengths, the number of pulses, and the relaxation time between pulses. These controls were then tested using the oscilloscope across the range of all expected parameters. The laser output was then verified to coincide with the controls.

Once controls were completed, investigation into triple pulsing could begin. It was determined (Ray Harp Ph.D. thesis, in preparation) blocked holes occur with two pulses while the third pulse cleans and clears the blind hole. This phenomenon guides straight to triple pulsing. Experiments were conducted using the most efficient pulse lengths determined in previous objectives. These results were then compared to previous findings.

The next step was to conduct an identical test to the three pulse test using ten pulses to investigate the effects of more pulses.

Pulsing frequency was then investigated using the ten pulse regime described. This experiment required pulsing the laser 10 times using three different frequencies. Ranging the capabilities of the laser, different pulsing frequencies were investigated.

Finally, the concept of group multiple pulsing was investigated. This entailed pulsing a single hole multiple times using single pulse. The same experiment was then conducted pulsing a single hole multiple times with groups of 10 pulses

6 Experimental Apparatus

The following experimental apparatus is based on the setup developed by Dr. Alex Paleocrassas for his Ph. D. thesis

A 300 W Ytterbium, Single-Mode, Fiber Laser (Figure 3.2-1) is used for this research. A NEMA two-phase 220V outlet provides electric power to the laser. Its near infrared (1,075 nm) beam is fiber deliverable and comes out of the collimator as a cylindrical 5 mm beam.



Figure 3.2-1: 300 W Ytterbium, single-mode fiber laser power unit

The laser beam quality is near Gaussian ($M_2 \sim 1.04$). An optical isolator (shown in Figure 3.2-2) was attached to the collimator and is used to divert any reflected light away from the

collimator in order to avoid damage to the fiber due the high reflectivity of aluminum. The beam diameter and beam quality were modified slightly (beam diameter ~ 7 mm, $M_2 \sim 1.15$).

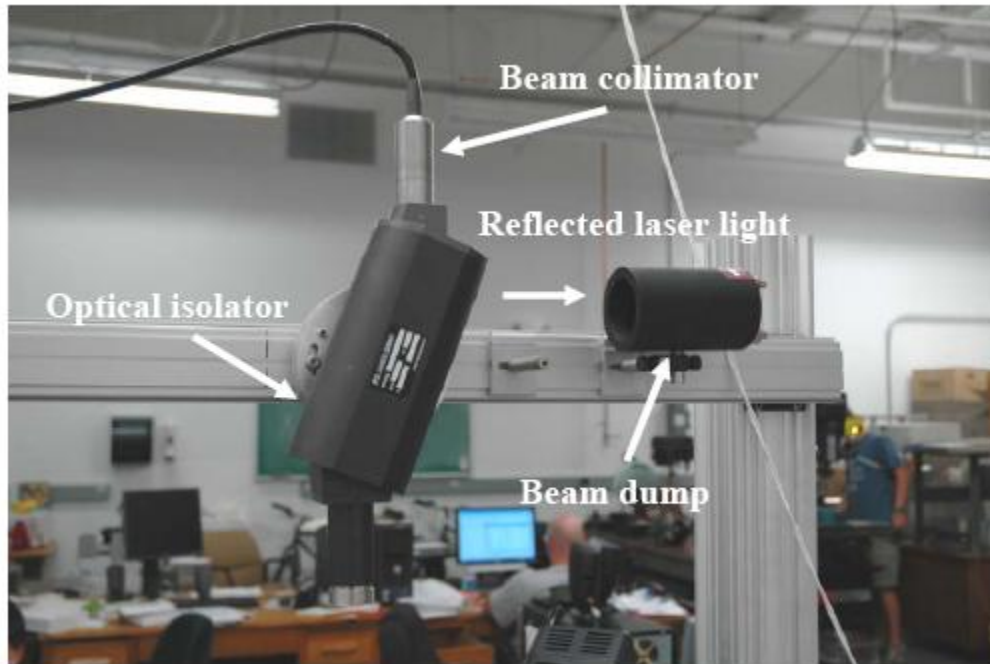


Figure 3.2-2 : Optical isolator connection to collimator, used to divert away reflected laser light into a beam dump

The Parker Automation X-Y linear motors (Figure 3.2-3) are used to move the work pieces and are controlled by the Galil X-Y axes motion controllers (Figure 3.2-4). The motors have a resolution of $.5 \mu\text{m}$ and a range of 1 m. The maximum acceleration and deceleration is ± 2 g's and maximum speed is 1.5 m/s.

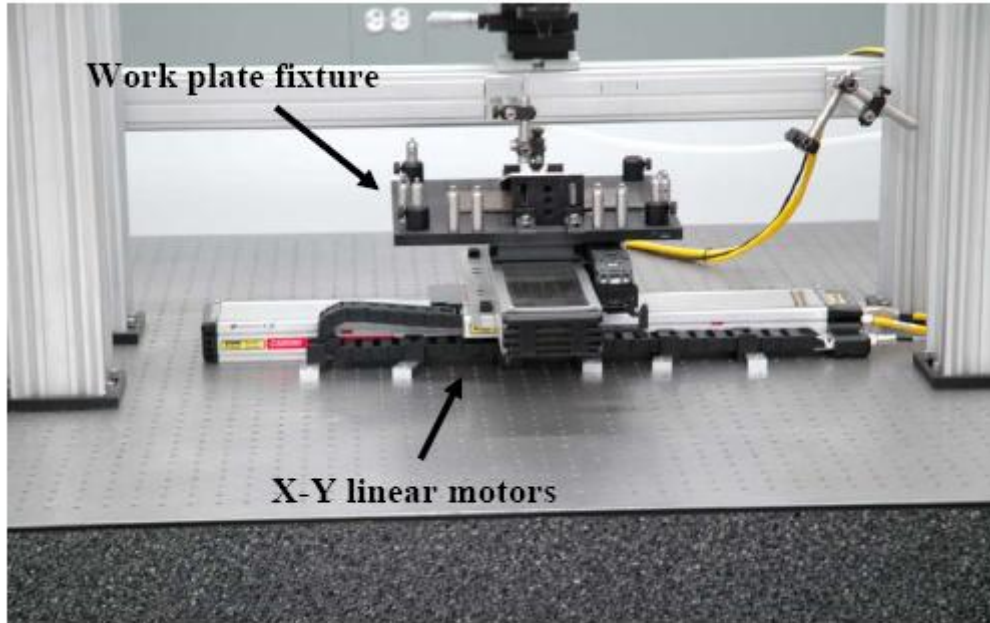


Figure 3.2-3: XY Linear motors with attached work plate fixture

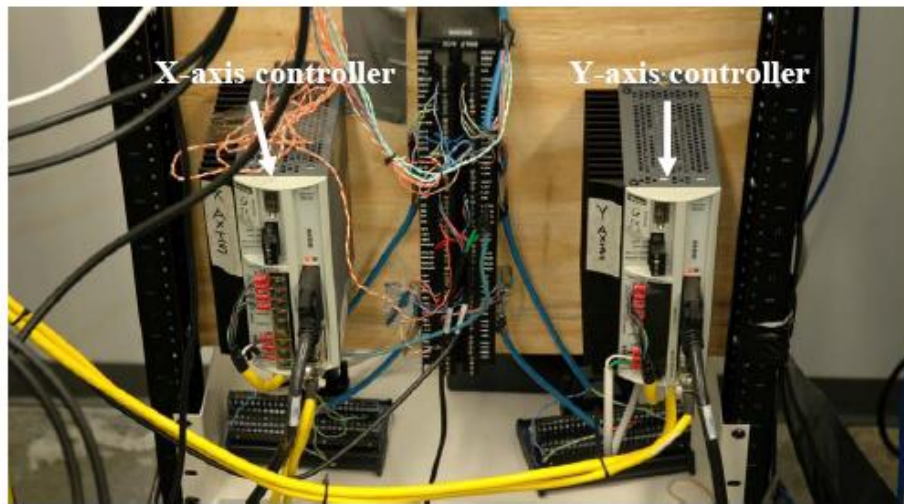


Figure 3.2-4: Galil X-Y axes motion controllers

The data acquisition system used is dSPACE 4.0 (Figure 3.2-5). It is mainly used as an external control for the laser and for acquiring data from sensors (photodiode). This helps automate the operation of the laser. Simulink is used to create different operation schemes and can be synchronized with the movement of the linear motors.

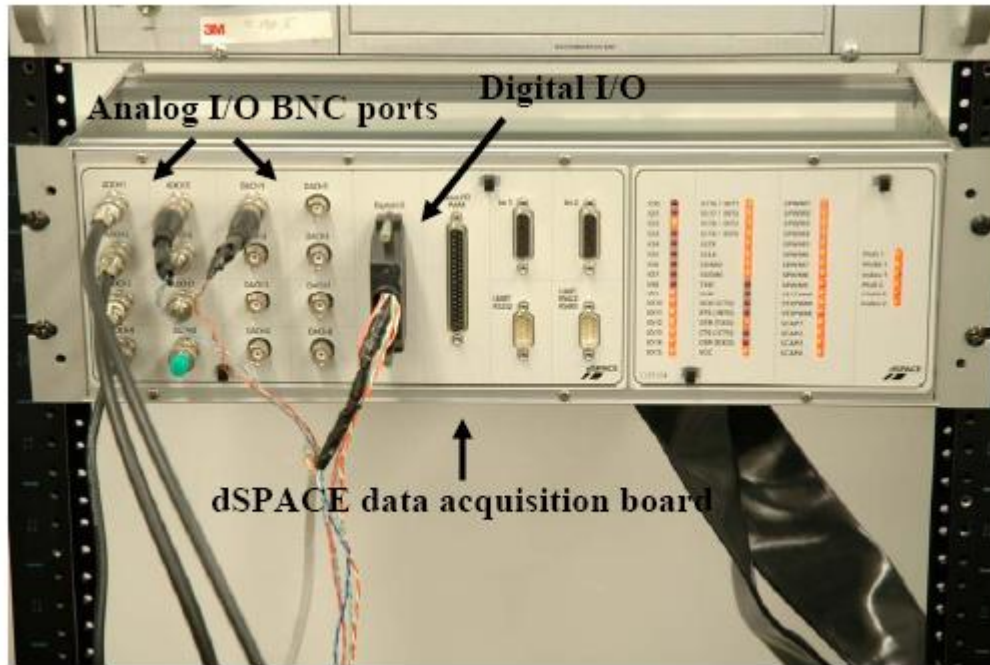


Figure 3.2-5: dSPACE 4.0 data acquisition system

A 3x beam expander is used in combination with the 100.1 mm OptoSigma triplet lens to obtain a minimum focus spot size of $12.01 \mu\text{m}$. Equation 6.1 shows how to calculate the minimum spot size.

$$\begin{aligned}
 \text{Spot Size} &= \frac{\text{Lens Focal Length}}{\text{Collimator Optics Focal Length} \times \text{Beam Expansion Factor}} \times \text{Fiber Diameter} \quad (6.1) \\
 &= \frac{100.1 \text{ mm}}{25 \text{ mm} \times 3} \times 9 \mu\text{m} = 12.1 \mu\text{m}
 \end{aligned}$$

Figure 3.2-6 shows the optical setup. The laser beam is centered with respect to the beam expander and the laser head. The laser head contains the focusing triplet and can be adjusted using the outer ring. At the bottom of the cutting head there is a chamber that allows for shielding to flow out through the welding nozzle. This chamber is sealed by a special cover glass and a rubber gasket.



Figure 3.2-6 : Beam expander and laser head setup

X, Y, Z Linear Micrometer Stages (Figure 3.2-7) are used to align the optics with the beam. Also, the Z stage is used to change the focusing of the beam, as well as the nozzle height with respect to the work piece surface. The resolution of the micrometer stages is $10 \mu\text{m}$ and their range is approximately 26 mm.

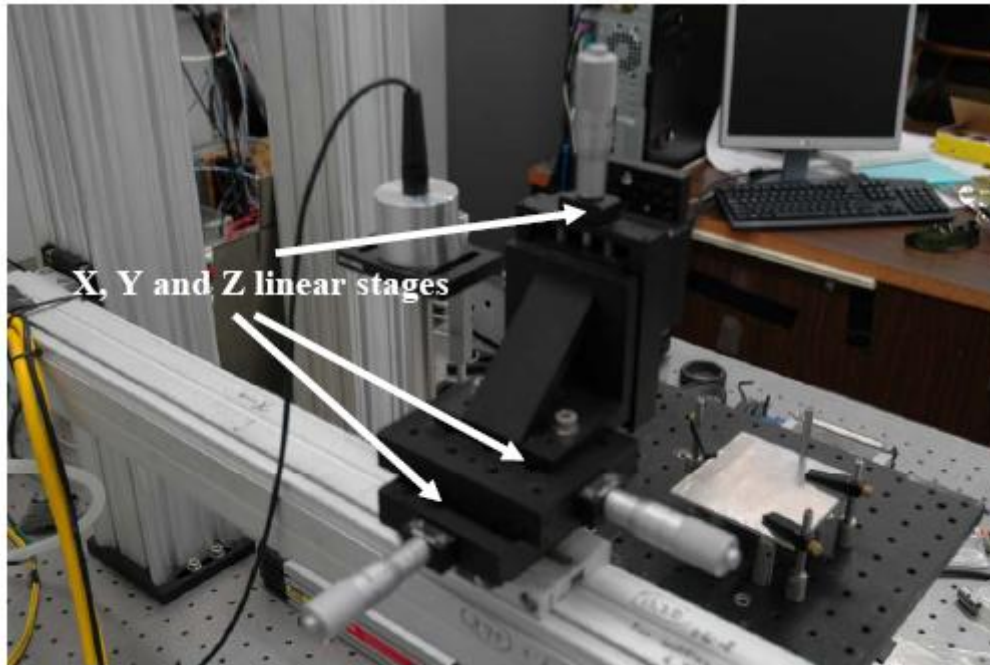


Figure 3.2-7: X,Y,Z micrometer linear stages

The laser is rated with a pulsing frequency up to 25 kHz. Control of pulsing can be done by two mechanisms: Digital circuitry and Analog circuitry. Inputs for the digital circuit are a single BNC connector used to control the modulation. The laser power is selected via the hand terminal supplied by the manufacturer. Depending on the signal supplied by the BNC connector, high or low, the laser will pulse in unison. Using the digital circuit, it is therefore necessary to create a signal mimicking desired pulse length and frequency.

Figure 1 in Appendix I shows the circuit designed using logic gates and 555 timers to create the desired pulses. Three timers control the process time, initial pulse length, and subsequent pulse lengths while logic gates are used for triggering. By changing the resistances on the 555 timers, the pulse lengths and process time can be manipulated. Also, a frequency generator, connected by a BNC cable, is used to control the frequency of pulses. Outputs are connected to BNC connectors for monitoring of the process time, the first pulse length, subsequent pulse lengths, and the overall output. Manual set and reset push buttons are connected as well as BNC connects for set and reset for computer control.

The analog circuit requires two inputs, U-control and TTL, via a 15-pin connector. Both signals must be high for laser pulsing. Power is adjusted via input signal from 0-10V, 10 V being 100% power. U-control is the modulation of pulses while TTL acts as an on off switch. Therefore, circuitry was designed to create a high TTL signal during the process time while modulation of U-control for pulse lengths and frequency. In order to complete this, additional circuitry was added to the original digital circuit. The analog circuit also requires a minimum 3 second U-control 'on' signal before pulsing begins.

Similar to before, logic gates and 555 timers regulate all the control. A 555 timer creates the 3 second required delay before TTL turns high. The TTL signal then starts the original digital circuit for pulse modulation. Again, the process may be started via push button or computer control. Outputs are again via BNC connections which are converted to 15 pin-connect for laser mating

All connects, resistances, and push buttons are organized on the front of the control box. On the user interface, the left side is for all input and output BNC connects. Three dials determined the resistance, and therefore time length, of the process time, initial pulse length, and subsequent pulse lengths, of the 555 timers. Located on the right hand side of the box are the manual buttons for set and reset for both the digital and analog circuits.

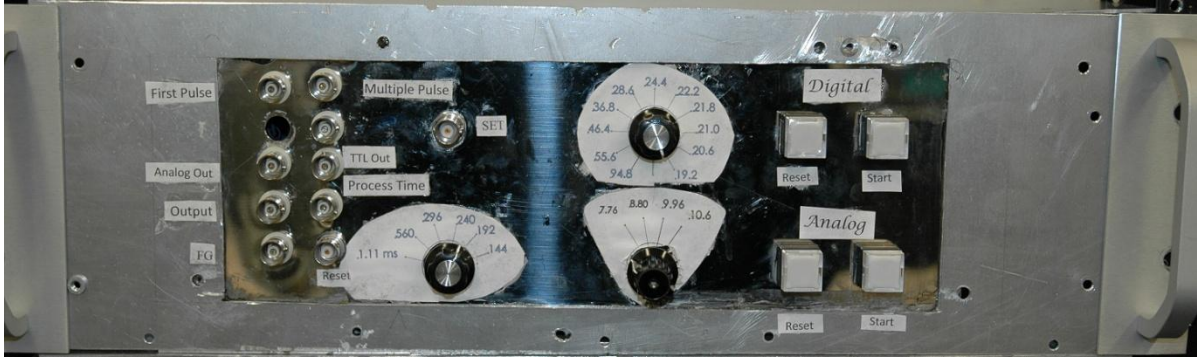


Figure 3.2-8: Circuit Control Box Interface

Figure 3.2-9 shows the circuit board created to control single and multiple pulses of the laser. On the far left are the input connects for set, reset, function generator, and time control resistances. The middle section of the board contains the timers and logic gates, and associated resistors and capacitors to complete the circuit. The far right has cable connects to the outputs for first pulse, subsequent pulses, process time, and overall output.

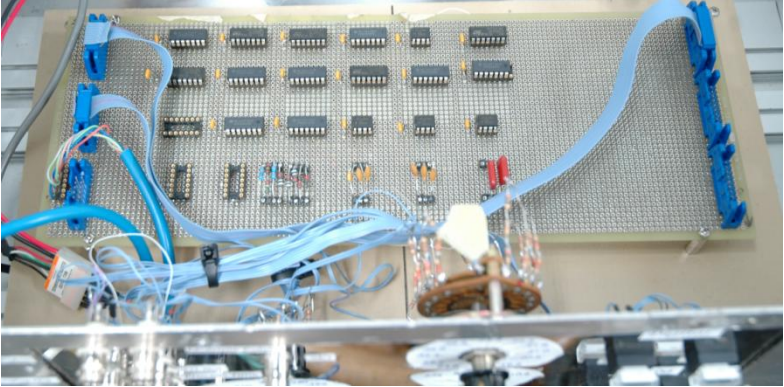


Figure 3.2-9: Circuit Board for Multiple Pulse Laser Control: Digital and Analog

For data acquisition, a Tektronix 3012B oscilloscope was used, shown in Figure 3.2-10. It has two input channels and the sampling rate capabilities go up to 100 MHz. It always acquires 10,000 samples and the sampling rate is determined by the time range that is chosen.



Figure 3.2-10: Tektronix 3012B oscilloscope

The Zeiss (Figure 3.2-11) inverted microscope was used to enlarge all the weld cross-sections and obtain pictures. There are a number of different magnifications that can be obtained. The current objectives are 2.5x, 8x, 16x, 40x and 80x. There is also an additional 2x magnification factor that can be multiplied to these aforementioned objective magnifications. Also, the eyepieces provide the user with a 10x magnification. Therefore, the maximum magnification that can be obtained is 1600x.



Figure 3.2-11: Zeiss Inverted Microscope

A Saphir 520 Grinder/Polisher (Figure 3.2-12) was used to polish the aluminum welds to a mirror finish. The grinding/polishing wheel can reach up to 600 rpm and 100 N of force can be applied to the samples. The grinding polishing head also spins at a constant 60 rpm and can be adjusted to spin clockwise or counter-clockwise.



Figure 3.2-12: Saphir 520 Grinder/Polisher

The vapor/plasma intensity measurements were obtained using a Hamamatsu silicon S1336-18BQ photodiode. This photodiode is most sensitive (80-90% transmission) in the visible spectrum, Figure 3.2-13. However, it also has moderate sensitivity (50-60% transmission) in

the near-infrared region which includes the wavelength of the laser (1,075 nm). In order to separate this signal during photodiode experiments a colored glass band pass filter was used that can filter out the reflected laser radiation.

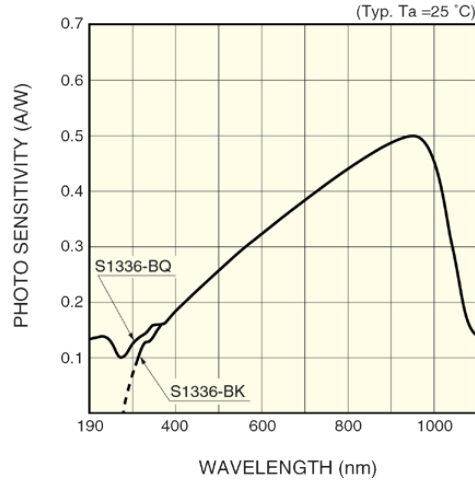


Figure 3.2-13: Hamamatsu Si S1336-B18BQ photodiode Spectral Response

The pulse waveform produced by the laser was measured using a Hamamatsu InGaAs Photodiode, G8370. The diode's sensitivity at the laser's 1,075 nm wavelength is ~ 75%, Figure 3.2-14. This, in addition to minimal sensitivity to visible light, was the major factor choosing it as a suitable diode.

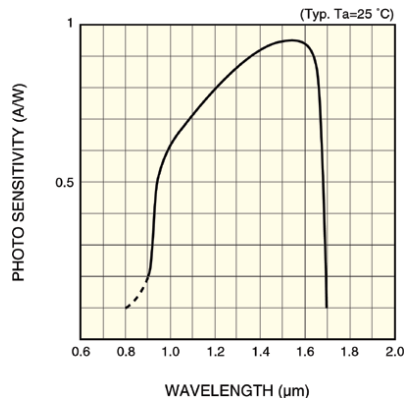


Figure 3.2-14: Hamamatsu InGaAs G8370 Photodiode Spectral Response

7 Experimental Procedures

All experiments and associated procedures are outlined below in order to better frame investigation methods. All apparatuses to which these instructions allude are described in detail in Section 6.

7.1 *InGaAs Photodiode Calibration*

Knowing the laser power output at peak levels is very important in order to better understand laser/material interactions. Power calculations were conducted using measurements by an infrared photodiode. Selection for the photodiode was based on laser wavelength and photodiode range. The selected photodiode will collect the 1075 nm wavelength while not being affected by recast and other light sources present. This allows for the reading of laser power only. Knowing the continuous wave (CW) laser output of 300W at full strength, a calibration curve for the photodiode was created as follows.

Steps for calibration of the photodiode are described below. Secure the photodiode directly below the laser to ensure optimal collection on the photodiode itself. Employ a 10 micron pinhole to reduce the incident intensity and ensure the photodiode does not become saturated. Pulse the laser for a duration of time allowing for the completion of the high initial spike and an appropriate amount of steady state output. Repeat this process for power percentages from 12.5% to 100% in 5% increments. Average the diode reading across the steady state and graph this against the known wattage from the laser. Plot these data and calculate a linear trend fit. This formula allows for the determination of any output power read by the diode during an experiment.

7.2 Focus Test

Precise focus of the laser beam allows for higher energy per unit area which in turn creates better hole quality via increased energy interaction. Optical focusing differs from that of theoretical calculations and therefore must be determined using the defined procedure below.

Steps for laser focus are described below and must be undertaken to ensure highest power to area ratio. Obtain and secure a sample of metal below the laser. Flatness of the sample is to be no greater than $\sim 0.0002''$ across the working area. Understanding the laser is a fixed height above the work table, it is only necessary to measure the surface height above the table. Once this is completed, find an extreme focal range by first placing the laser nozzle on the metal. Increase the distance between the laser nozzle and the sample surface in .5 mm increments, firing the laser each time, until a faint spark is seen. After the initial spark, reduce increments to .01 mm until the spark grows strong and eventually fades. Measure hole diameters and plot them against the distance between the nozzle and the sample surface. A 2nd order polynomial trend line will reveal the focus position, at which the hole diameter will be at a minimum.

7.3 Single Pulse Test

The phenomena associate with single pulse ablation are tested and investigated once laser power and focusing position have been established. During these tests, the ejected plasma intensity was measured simultaneously. Procedures for plasma measurement are found in Section 7.5 should be followed and setup in order for cohesive testing.

Steps to complete single pulse test are described below. Secure a sample under the laser ensuring less than $\sim 0.0002''$ flatness across the working area. Set up the control module to create a single pulse of desired length. Pulse the laser moving the sample in between pulses, creating as many holes as required.

7.4 Multiple Pulse Test

Further investigation required the sample to be ablated by multiple pulses. Completion of this task requires the control box outlined in Section **Error! Reference source not found.** gain, plasma measurements are to be taken during this process and section 7.5 should therefore be read and followed during this procedure.

An outline of how to conduct a multiple pulse test is described below. Secure a sample under the laser ensuring less than $\sim 0.0002''$ flatness across the working area. Set up the control module to create a multiple pulse sequence with desired initial pulse length, subsequent pulse lengths, and relaxation time between pulses. Pulse the laser ensuring the sample only moves once all pulses are complete.

7.5 Plasma Measurement

Plasma measurements were recorded in time with all pulse drilling experiments conducted. Plasma intensities show laser/material interactions that can be linked to pulse energies.

Methods for measuring the plasma formation intensities were conducted as follows. Fit a Nikon D70 camera with a 1336 Si photodiode so that the focusing and orientation of the camera viewfinder aligns the photodiode with the drilling position. Additionally, fit a high-pass filter to the camera lens to block the transmission of visible light. Place a second photodiode, InGaAs diode G8370, at the beam splitter to measure the laser pulse, as well as act as a trigger for the collection of data. Open the camera shutter manually during the experiment. Both photodiodes are connected to the oscilloscope using the beam measurement as the trigger.

7.6 *Sample Grinding/Polishing*

Microscopic views of holes and sample integrity must be obtained in order to fully investigate the effects of laser ablation on the material. Because of this, the sample must be ground and polished to reveal not only hole characteristics but metal microstructure. Below are the steps employed to grind and reveal holes created in both the single and multiple pulse tests.

Described below is the procedure to grind and polish a sample for microscopic viewing. Excess material must be removed in order for the sample to fit in the molds for resin setting. A retaining clip is attached to the sample in order for proper alignment in the mold. After mixing the resin, as outlined by the supplier, the resin is poured into the mold and allowed to cure. The sample is then removed and placed in the grinder. Depending on removal rate desired, the correct grinding surface is to be chosen. After setting appropriate time, force, rotational speed, and grinding technique, activate the grinder. Once complete, remove the sample and view using the microscope. Higher finishing requirements will require more iterations of the above procedure using smoother and smoother finishing cloths.

8 Results and discussions

Initial baseline results were first determined to ensure repeatability and proper functioning of laser set-up in comparison with earlier investigation. Baseline results as well as digital/analog comparison for single pulse micro-hole drilling are presented in Section 8.1. These results are followed by the findings concerning three pulses, ten pulses, power densities, and pulsing frequency; Sections 8.3, 8.5, 8.6, and 8.7. Sections 8.2 and 8.4 detail the process anatomy of both single and multiple pulse ablation. Finally, Section

8.1 Single Pulse Results

Before multiple drilling experiments commenced, single shot drilling was investigated. Experimental data necessary to move onto future experiments included determining the optimal pulse length for single shot ablation, the aspect ratio of a single shot hole, the and the plasma ejection trends.

The optimal pulse length experiment, with pulses ranging from 1 μs to 10 μs , determined the highest aspect ratio hole created occurs at a laser pulse length of $\sim 3\mu\text{s}$, requiring a control signal of 26.2 μs . Figure 8.1-1, as measured by correlating photodiodes, depicts the control signal and the laser pulse.

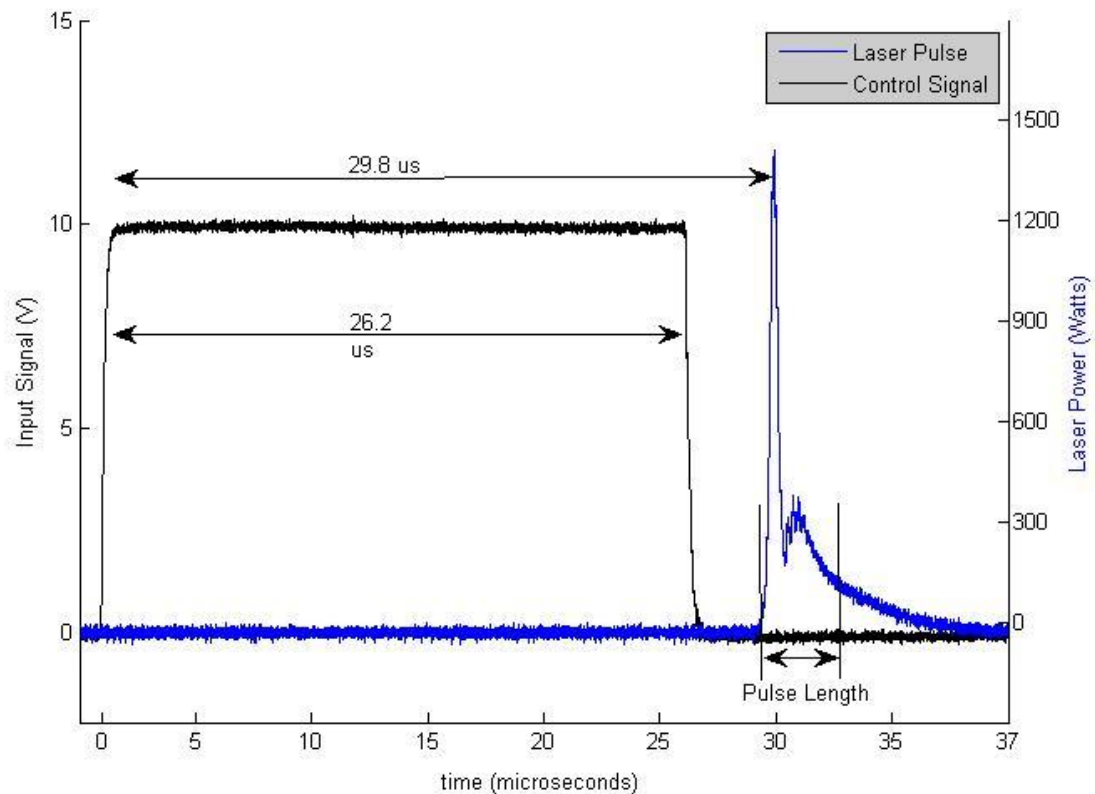


Figure 8.1-1: Input Pulse and associated Pulse Waveform for Single Pulse

Consistently, there is a clear delay between the control signal and the laser output of $\sim 2.5 \mu\text{s}$. The laser output reaches its maximum strength, $\sim 1470 \text{ W}$, and quickly trails off with minimal steady state input. This emits the maximum energy in the least amount of time.

This pulse is consistent with experiments conducted earlier⁽³⁶⁾. A change has occurred, however, in the optical alignment and focusing techniques of operation. Because of this, single pulse testing was conducted to act as a baseline for future experiments and comparison to previous findings.

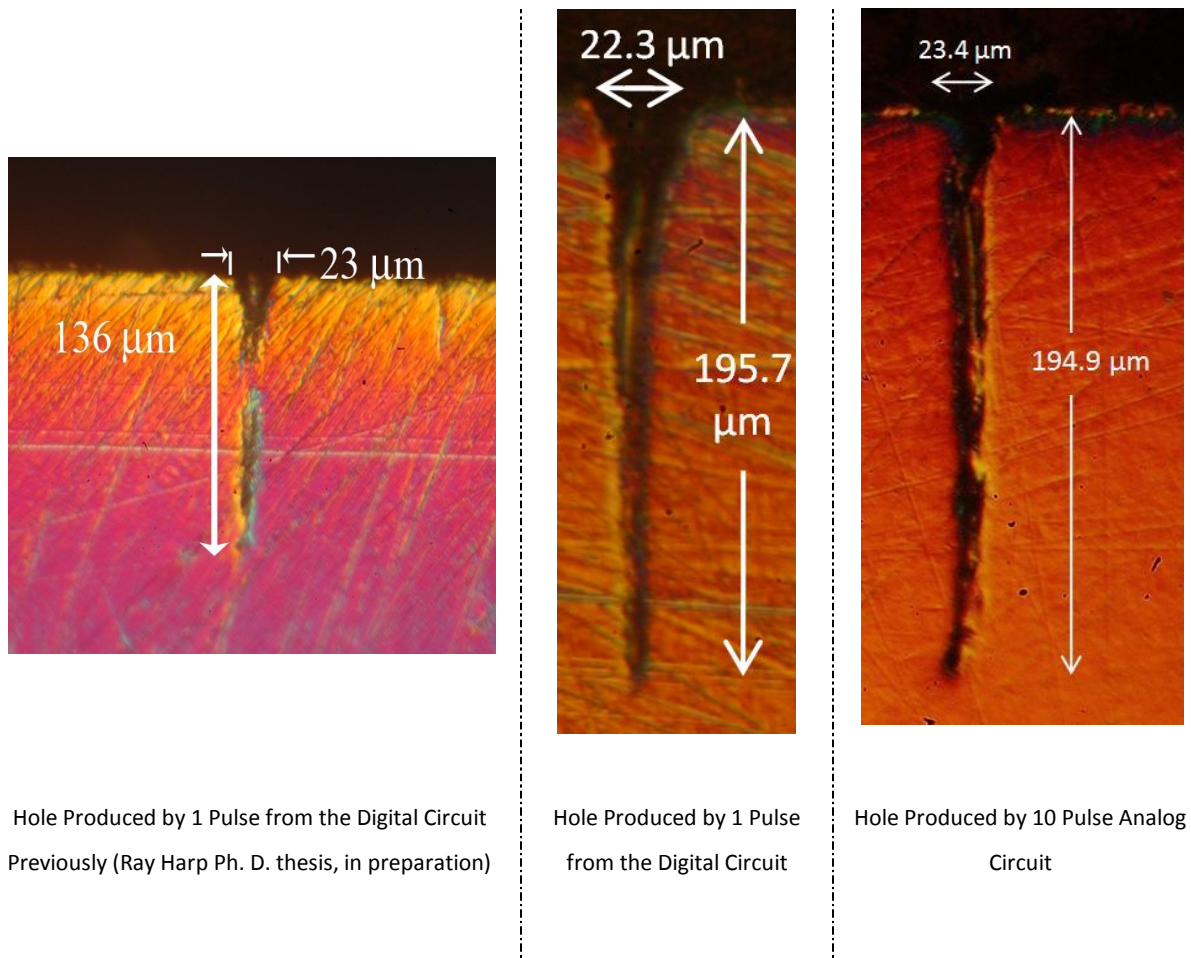


Figure 8.1-2: Hole Profiles Produced by 1 Pulse

Above is a comparison of the results from previous tests, results from the current set-up through the digital circuit, and results through the analog circuit. The increase in depth of nearly 60 microns from previous work can be attributed to improved optical alignment and improvements in focusing techniques and control. Currently, whether using the digital or analog circuit, hole depths are ~ 195 microns with diameters ranging between 22- and 24 μm . Hole aspect ratios ~ 6 are expected using the current set-up under single pulse ablation. Also of note is the clear hole produced. Previous work experienced blockage after a single pulse

which is no longer present. The clear blind holes can be attributed to better focus which creates higher power densities on the sample. This leads to higher plasma temperatures, higher pressure shockwaves, and therefore more violent and energetic ejection.

Plasma intensity results obtained show plasma formation and ejection lags behind the onset of the radiation by $\sim .2 \mu\text{s}$. Plasma intensity rises with laser intensity reaching a peak between 600- and 800 μs . The plasma intensities fall to zero $\sim 3\mu\text{s}$. Figure 8.1-3 also leads to the conclusion that plasma intensity is directly correlated to laser power, agreeing with results from earlier experiments (Ray Harp Ph. D. thesis, in preparation).

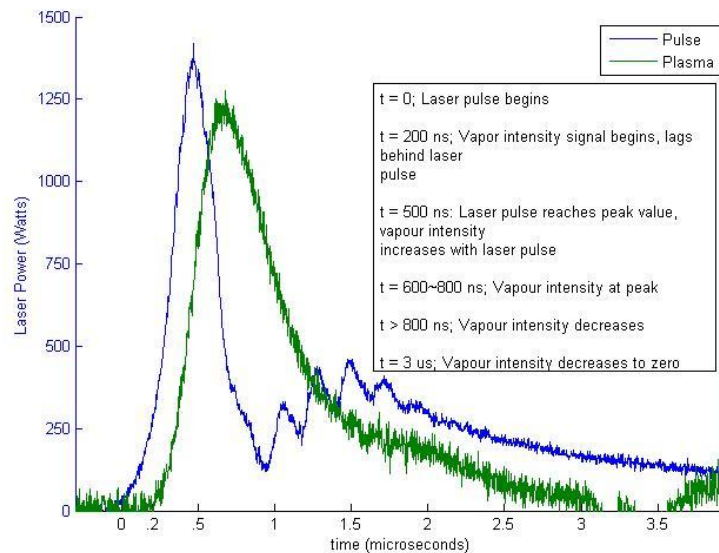


Figure 8.1-3: Plasma ejection of a Single Pulse on Steel

8.2 Process Anatomy of Single Pulse

The process of single pulse ablation can be broken into four distinct time intervals. Each interval relies on different mechanisms for material removal and ejection. Figure 8.2-1 shows the four steps with descriptions of laser-material interaction to follow.

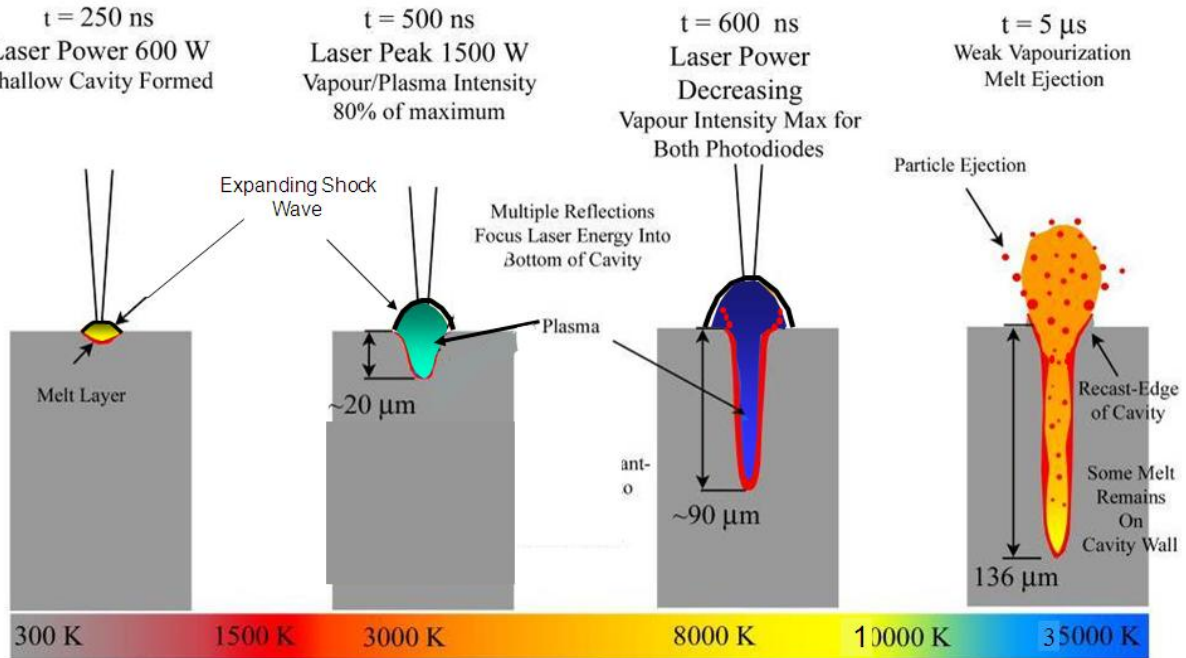


Figure 8.2-1: Process Anatomy of Single Pulse Ablation

Step 1: The high initial spike, ~ 1500 W, creates an environment modeled by a semi-adiabatic evaporation in which a significant amount of solid is removed. The high amounts of energy are, due to the semi-adiabatic nature, absorbed by the evaporated material creating hot plasma between 16,000 K and 70,000 K.

Step 2: The high temperature plasma creates an expanding shockwave in the surrounding air. Meanwhile, a keyhole is formed as material continues to evaporate and change phase into plasma.

Step 3: The hole depth begins to rapidly grow as plasma is ejected while the laser further heats the cavity bottom as it is reflected downward off the walls. At this point, both high temperature ablation and adiabatic evaporation assist in material removal.

Step 4: The hole depth now requires the laser to be reflected multiple times before interacting with the bottom of the cavity. These reflections deposit energy into the walls of the cavity. Walls are therefore widened and the laser energy is dramatically reduced as it penetrates into the cavity. The reduction in energy intensity allows the plasma to cool, creating significant melt both along the walls and at the bottom of the cavity. Eventually, after the pulse has finished, the plasma cools to hot melt and saturated vapor as it leaves the cavity. This process leaves melt and recast in and around the cavity after the process is completion, $\sim 150 \mu\text{s}$. If a second pulse is irradiated after $150 \mu\text{s}$, energy will be used to reheat the material thus lowering the process efficiency.

In this thesis the ability, much in comparison to recent experiments ⁽³⁴⁾⁽³⁵⁾, to deposit subsequent pulses before solidification occurs will be explored. By maintaining high vapor temperatures in the hole, high material removal rates and efficiencies in energy deposition are sought.

8.3 Triple Pulse Results

The realm of micro-hole drilling extends far beyond the 200 μm depths capable by a single pulse. Requirements call for holes much deeper, and the following researched the effects multiple pulses have on micro-holes in steel. Experiments were conducted to demonstrate the difference between one, three and ten pulses on a substrate.

Below, Figure 8.3-1, shows the correlation between the control signal and the laser's output. With control signal pulses spaced an equal 77 μs apart, the laser output is irregular. The time between the first and second pulses is shortest while all subsequent pulses align with the control signal.

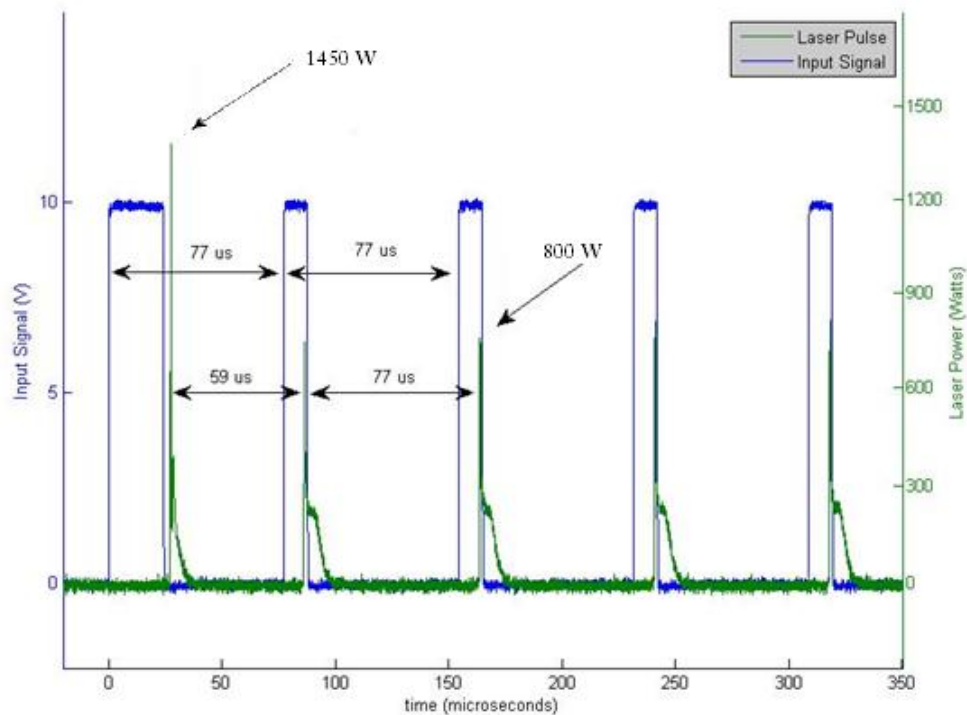


Figure 8.3-1: Input Signal and Laser Pulse of Multiple Pulses

The above findings in pulse spacing are consistent across frequencies in later experiments. The input signal will therefore not be addressed for each individual experiment.

The laser pulse of the digital circuit as captured by the photodiode is pictured in Figure 8.3-2. As shown, the initial pulse retains the high spike while the subsequent pulses, although not as high, exhibit initial spikes in power. These results are for the digital circuit at 13.1 kHz. The analog circuit, as shown in Figure 8.3-3, is nearly identical to the digital circuit with the exception of strong peaks in power. The second pulse has no peak while the third pulse's peak power is not as strong as the digital circuit.

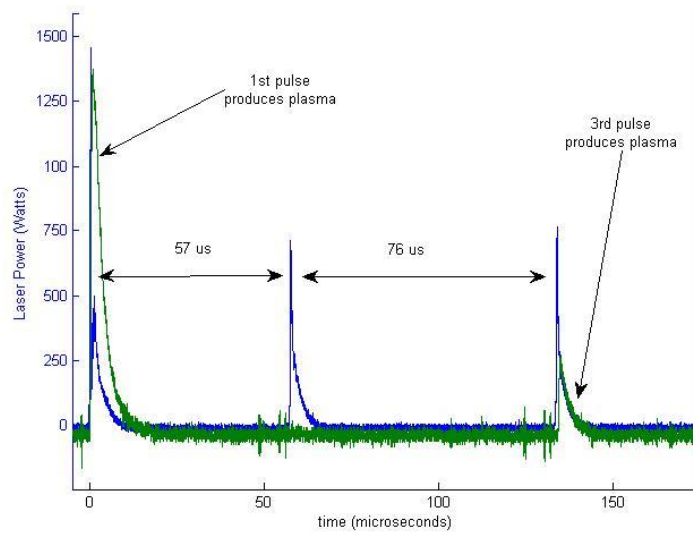


Figure 8.3-2: Pulse Waveform and Plasma Intensities of 3 Pulse Digital Circuit

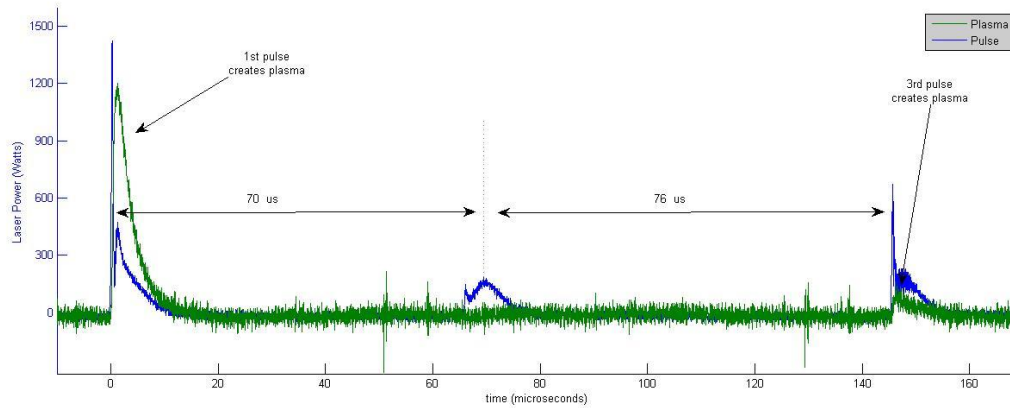
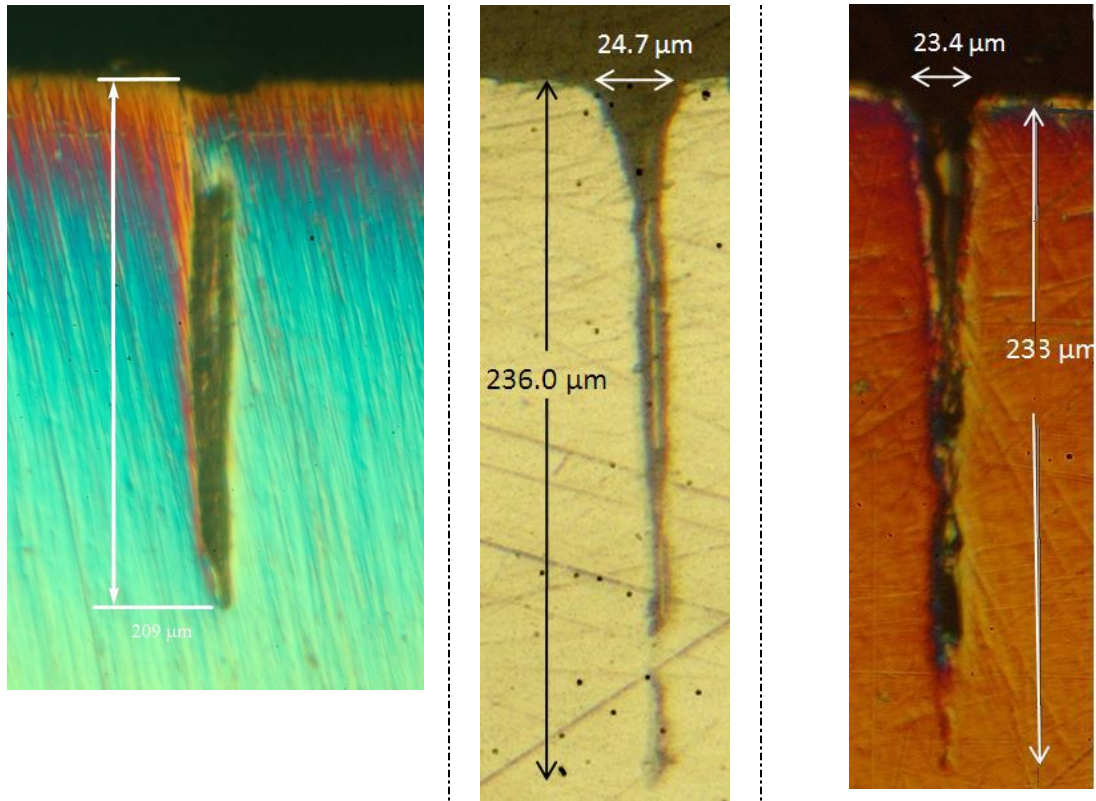


Figure 8.3-3: Pulse Waveform and Plasma Intensities of 3 Pulse Analog Circuit

More detailed explanations of material removal can be deduced from the plasma measurements, which are similar in trends. The extreme irradiative flux on the material by the initial spike creates high intensities of plasma as depicted by the green line. No plasma is produced on the second pulse. The third pulse, once again, shows sign of plasma ejection. This phenomenon is due to rising plasma in the hole re-solidifying between the second and third pulses. The third pulse then frees the solidified material and ejects it in the form of plasma.



Hole Produced by 3 Pulses from the Digital Circuit Previously

Hole Produced by 3 Pulses from the Digital Circuit

Hole Produced by 3 Pulses from the Analog Circuit

Figure 8.3-4: Hole Profiles Produced by 3 Pulses

Above, improvements in the 3 pulse paradigm from earlier work are shown. An increase of $\sim 30 \mu\text{m}$ is consistently ablated using the improved optics and focus. Currently, the analog and digital circuits are nearly identical in depth and width. Typical hole depths are captured in Figure 8.3-4. Aspect ratios of 3 pulses at 13.1 kHz are ~ 10 . This indicates an increase of nearly $40 \mu\text{m}$ in depth created by the two secondary pulses. Slight hole blockage is beginning to occur as shown towards the bottom of the crevices.

8.4 Process Anatomy of Multiple Pulses

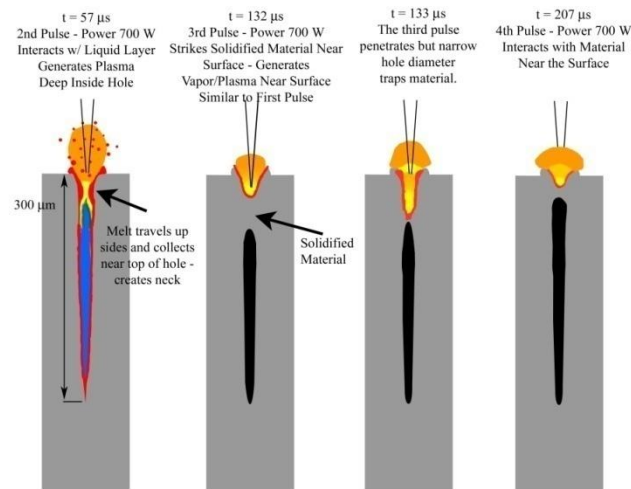
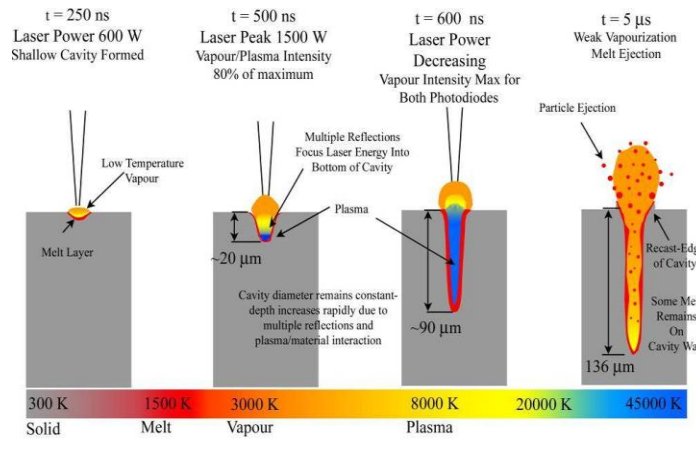


Figure 8.4-1: Process Anatomy of Multiple Pulse Ablation

Stages 1-4: Multiple pulse drilling begins with the same pulse as described in single shot ablation. The process begins by semi-adiabatically evaporating material and superheating it into plasma. The hot plasma creates a pressure difference ejecting material. As the laser power decreases and the plasma begins to cool, hot melt and vapor ejects from the hole.

Stage 5: It is known plasma is still present in the hole at 57 μs after the pulse completes. The second pulse begins within this timeframe and thus interacts with the high temperature material still present. Increases in absorption further increase the depth on the hole. As the walls melt, the material begins to move up the cavity beginning to solidify near the top of the hole. Eventually the solidifying material blocks the hole.

Stage 6: The subsequent pulse melts and vaporizes the newly formed blockage near the hole's entrance. As the hole is cleared, the laser's energy will again reflect down the cavity creating vapor and melt to both widen and deepen the hole.

8.5 Ten Pulse Results

Next, the sample was ablated with ten pulses at 13.1 kHz to compare with the 1 and 3 pulse schemes. The laser pulse waveform is depicted in Figure 8.5-1 for the digital circuit and Figure 8.5-2 for the analog circuit. Consistent with the 3 pulse output, the first spike, for the digital is roughly double the subsequent pulses.

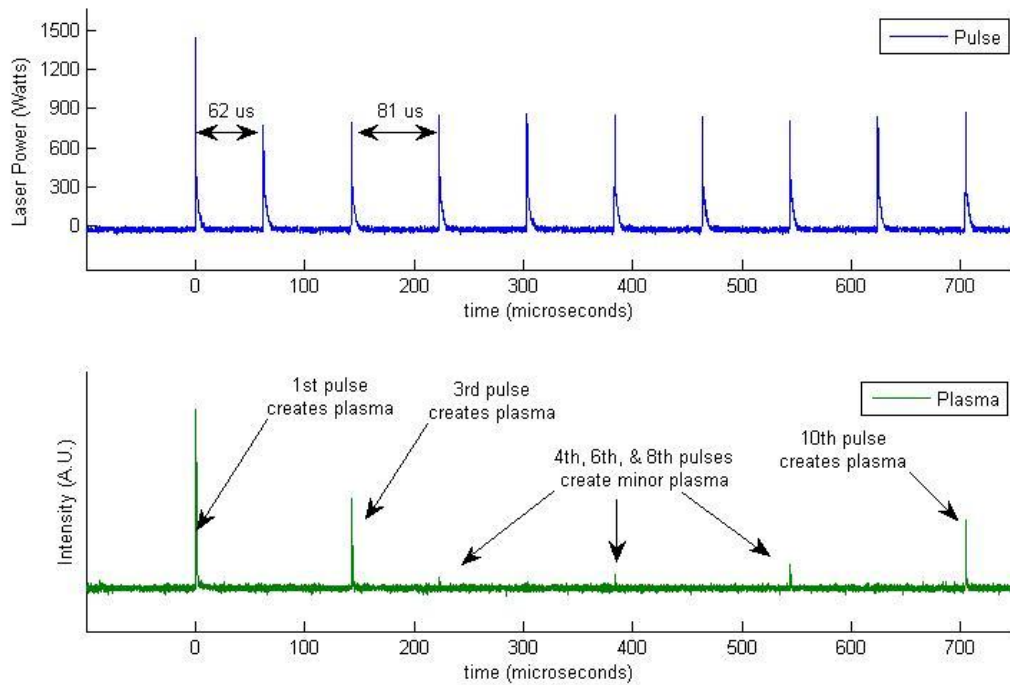


Figure 8.5-1: Pulse Waveform and Plasma Intensities of 10 Pulse Digital Circuit

The analog circuit again lacks a power spike on the second pulse and subsequent pulses. Because of this no plasma ejection is experienced throughout the ten pulses.

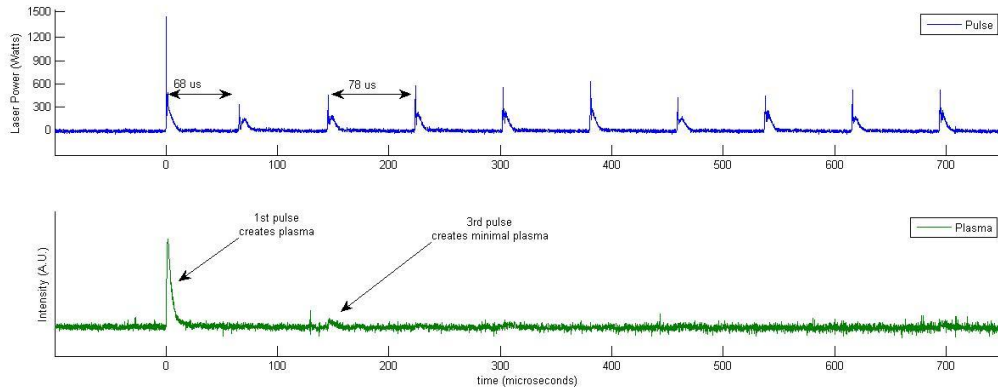
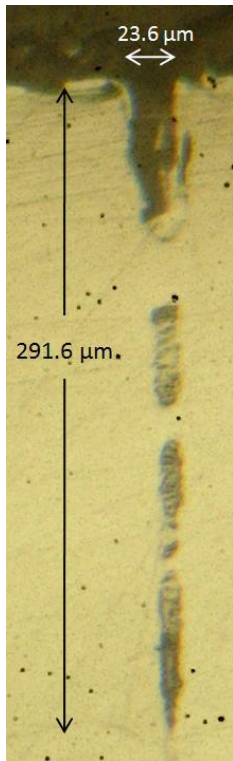


Figure 8.5-2: Pulse Waveform and Plasma Intensities of 10 Pulse Analog Circuit

Plasma ejection intensities were measured and are similar to 3 pulses. Figure 8.5-1 shows high initial plasma. Later plasma ejection occurs again at 3 pulses, consistent with earlier results. Although the digital circuit continued to form plasma as the pulsing continued the analog circuit lacked sufficient power. Applying this to Figure 8.5-3, conclusions may be drawn about the wider, more blocked hole created by the analog circuit. With different power densities, the energy imparted on the piece is still comparable between the two circuits. The comparable depths of holes imply the energy imparted is the important aspect to hole depth after the initial pulse. The digital circuit experienced less blockage due to the higher power spikes which created plasma for more energetic escape.



Hole Produced by 10 Pulses from the Digital Circuit



Hole Produced by 10 Pulses from the Analog Circuit

Figure 8.5-3: Hole Profiles Produced by 10 Pulses

The nearly identical pulse waveform as shown earlier creates comparable holes between the digital and analog circuits. Depths nearing 300 μm are photographed with aspect ratios ~ 12 . The increased depth creates the problem of molten material re-solidifying in multiple locations on the edges of the hole before exiting.

A graphical representation of hole depth due to number of pulses for both the digital and analog circuitry is shown in Figure 8.5-4. The correlation between the two circuits is high with large increases in hole depth for the first pulse followed by declining benefits per pulse as the number increases. No real difference between the two circuits is present at 13.1 kHz.

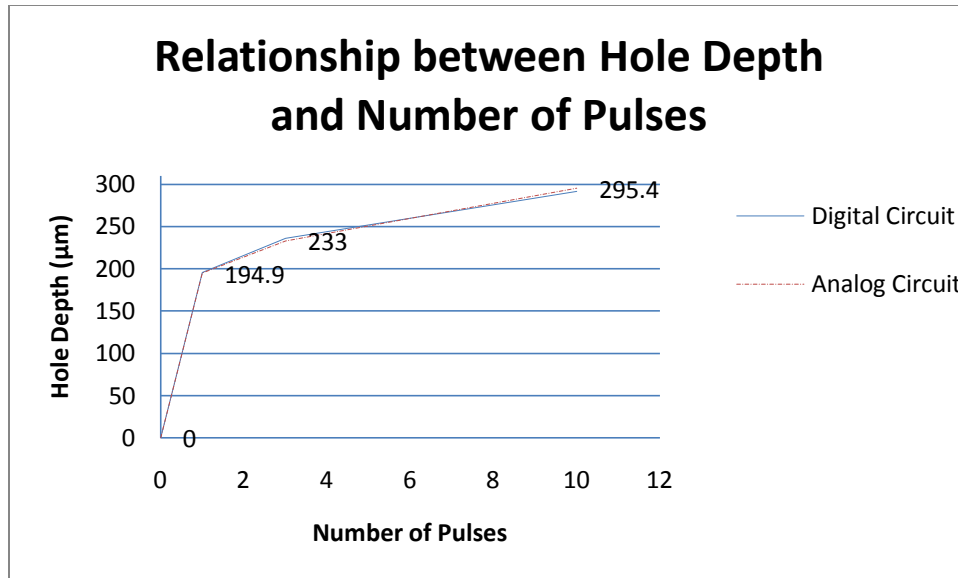


Figure 8.5-4: Relationship between Hole Depth and number of Pulses

Of interest is the material removal rate as the number of pulses increases. The initial pulse removes ~ 200 microns. The following two pulses increase the depth nearly 20%. The following 7 pulses only deepen the hole 25%. This shows a drastic drop in material removal per pulse at pulse numbers greater than 3. Also of note is the hole blockage occurring with the increase of depth beyond a 240 microns. This blockage is explained by a lack of sufficient kinetic energy to exit the hole. The initial pulse, as exhibited by all pulse graphs, shows extremely high initial power. This is required to overcome reflection at the surface and create a keyhole at the site of pulsing. The extreme power density creates high temperature plasma exiting away with high pressure. Subsequent pulses lack this power density and the escaping vapor no longer has efficient energy to exit the hole, creating blockage. There is a finite depth between 240 microns and 330 microns at which the hole will reach a maximum depth while remaining unblocked.

8.6 Effects of High Initial Power Density

The major difference between the digital and analog circuits occurs at 16.1 kHz. At this frequency, the analog circuit no longer produces high power spikes at the onset of pulses. Digital circuitry retains this phenomenon until nearly 20 kHz. This discrepancy will show the effect the high power density has on hole creation. The following tests were conducted using the digital and analog circuitry for comparison. The laser was pulsed 10 times at a frequency of 16.1 kHz.

The single difference in laser output on the digital side is the spike of the second pulse. At higher frequencies, the second pulse's spike fades. 16.1 kHz produces a spike at 50% of the original strength. This does not affect results as conclusions will be drawn about the effects of the spikes. All other pulses retain the high spike. In corroboration with earlier plasma measurements, the first and third pulses create plasma ejection while plasma is later ejected as well.

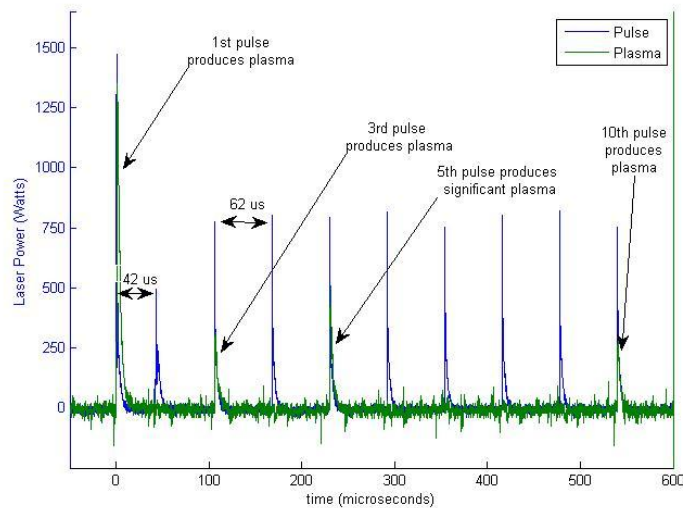


Figure 8.6-1: Pulse Waveform and Plasma Intensities of 10 Pulse Digital Circuit at 16.1 kHz

Trends of the analog circuit at 16.1 kHz are shown below. Most notably, the initial spike still has a sharp rise while all subsequent pulses reach the laser's steady state output, Figure 8.6-2. Pulses are wider than the digital circuit at the same frequency. Also, the pulses' peak intensity falls slightly behind that of the digital circuit.

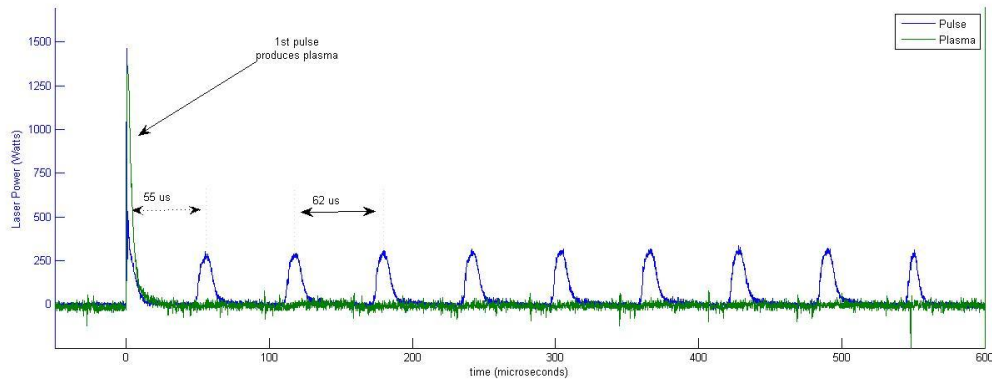
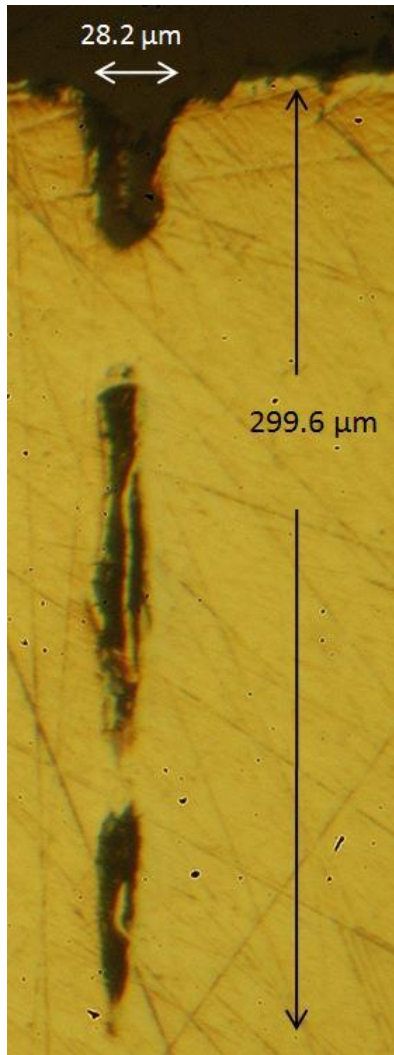


Figure 8.6-2: Pulse Waveform and Plasma Intensities of 10 Pulse Analog Circuit at 16.1 kHz

Vapor intensities show ejection created only by the first pulse, Figure 8.6-2. The lack of high power spikes weakens the laser's ability to produce plasma. The digital circuit maintains power spikes, and therefore plasma creation. This ability leads to cleaner holes as illustrated by Figure 8.6-3. The energy inputted is nearly equal for both circuits, and therefore the hole depth is comparable.



Hole Produced by 10 Pulse Digital Circuit at 16.1 kHz



Hole Produced by 10 Pulse Analog Circuit at 16.1 kHz

Figure 8.6-3: Hole Profiles from 10 pulses at 16.1 kHz

Results shown above, Figure 8.6-3, show the high power density spike affects the hole in two ways; depth and width. The digital side, retaining the power spike, created a hole narrower and deeper than the analog circuit. This is explained by higher plasma and vapor temperatures maintained during digital pulsing. The lower power densities experienced

during analog pulsing leads to cooler temperatures, increased melt, and less energy for material removal. This is witnessed by increased blockage, minimal plasma ejection, a wider diameter. The digital circuit maintained the ability for high temperature plasma and thus ablated cleaner holes. Energy of both schemes is similar and therefore, no advantage is seen in hole depth.

Comparing the digital results to those obtained by 10 pulses at 13.2 kHz, the increased frequency also increased the hole depth to 299 μm . This implies imparting energy quicker and maintaining higher temperatures within the hole makes the process more efficient. More detailed insight into the effects of frequency can be found in Section 9.7.

With the digital side capable of creating cleaner holes due to higher power spikes, it should be used up to ~ 20 kHz due to the retention of high power spikes.

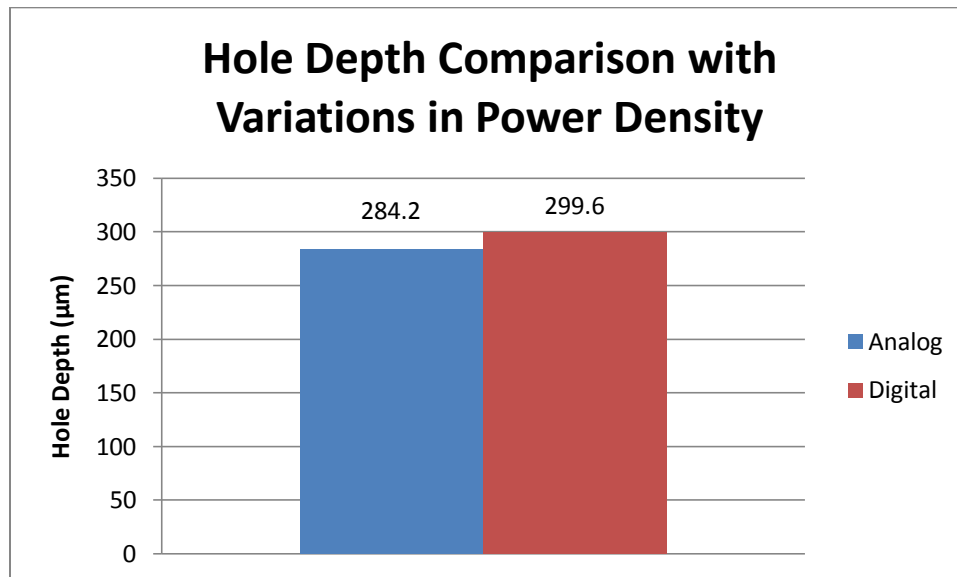


Figure 8.6-4: Hole Depth Comparison with variations in Power Density of 10 Pulses at 16.1 kHz

With no major change in depth, graphically represented by Figure 8.6-4, it is apparent the power spikes of subsequent pulses do not greatly affect the outcome of the hole. This result shows the importance of the high initial power density followed by a consistent pulsing of energy to expel vapor. The high density created by the first pulse creates the plasma and key hole necessary for extremely high material removal. Subsequent pulsing spikes lack this extreme power density. Their energy input therefore becomes the major factor effecting material removal. The pulse energy enters the hole heating the vapor as it exits the hole. As with the 13.1 kHz results, energy still is not sufficient to overcome the height and some vapor is caught in the hole as it cools and solidifies.

8.7 Effects of Pulse Frequency

Seeing from the above results, an increase in frequency increased hole depth. Results below investigated the limits of the laser's frequency and the effects it has on micro-hole drilling. In particular, the digital circuit was pulsed for ten pulses at 31.5 kHz, 42.8 kHz and 48.7 kHz.

Again, the pulse waveform was recorded by the photodiode and is shown for 31.5 kHz in Figure 8.7-1. Consistent still is the initial power spike followed by 9 pulses reaching the laser's steady state output. In addition to dramatically reducing time intervals between pulses, the laser no longer exhibits signs of high power spikes.

The lack of plasma during the later 9 pulses indicates material is continuously evaporated and ejected. This explains the extreme blockage near the hole's exit occurred after pulsing was complete.

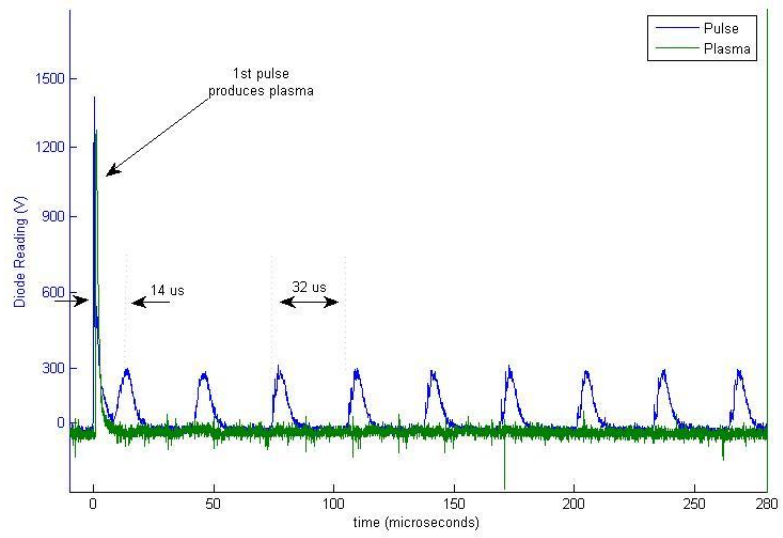


Figure 8.7-1: Pulse Waveform and Plasma Intensities of 10 Pulses at 31.5 kHz

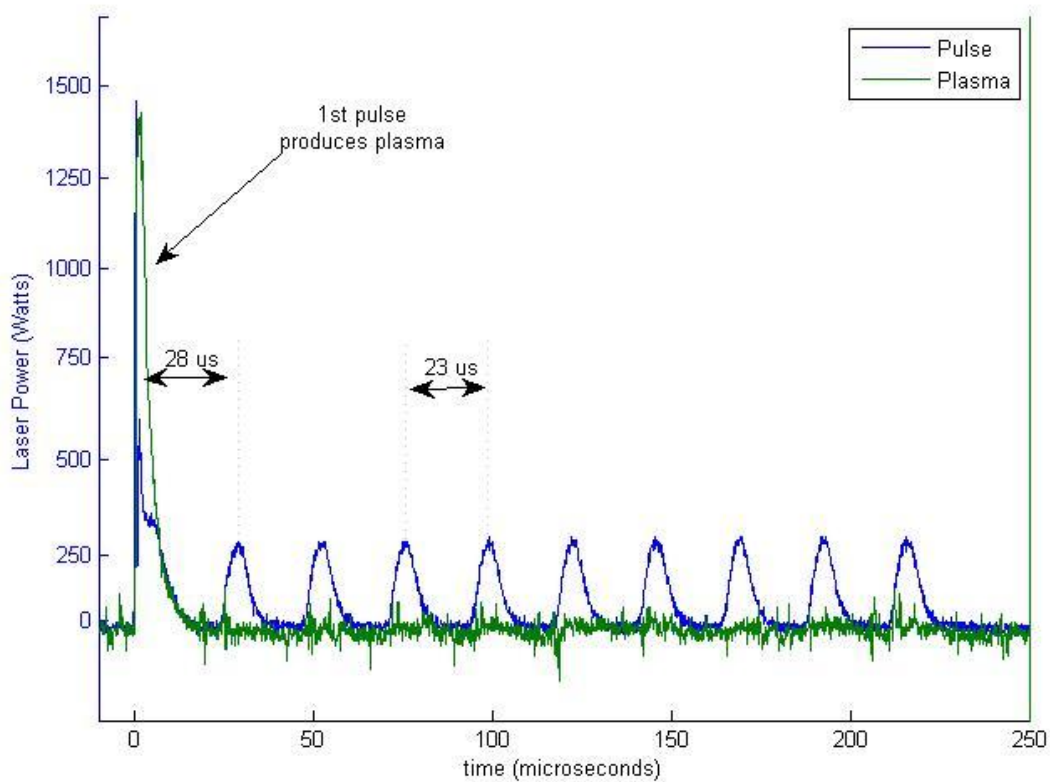


Figure 8.7-2: Pulse Waveform and Plasma Intensities of 10 Pulses at 42.8 kHz

The pulsing frequency was increased to a medium repetition of 42.8 kHz. The laser output is consistent with earlier results and is pictured in Figure 8.7-2. One anomaly present is the longer initial pulse length. This is in fact due to the second pulse, forced by increased frequency, interacting with the initial pulse.

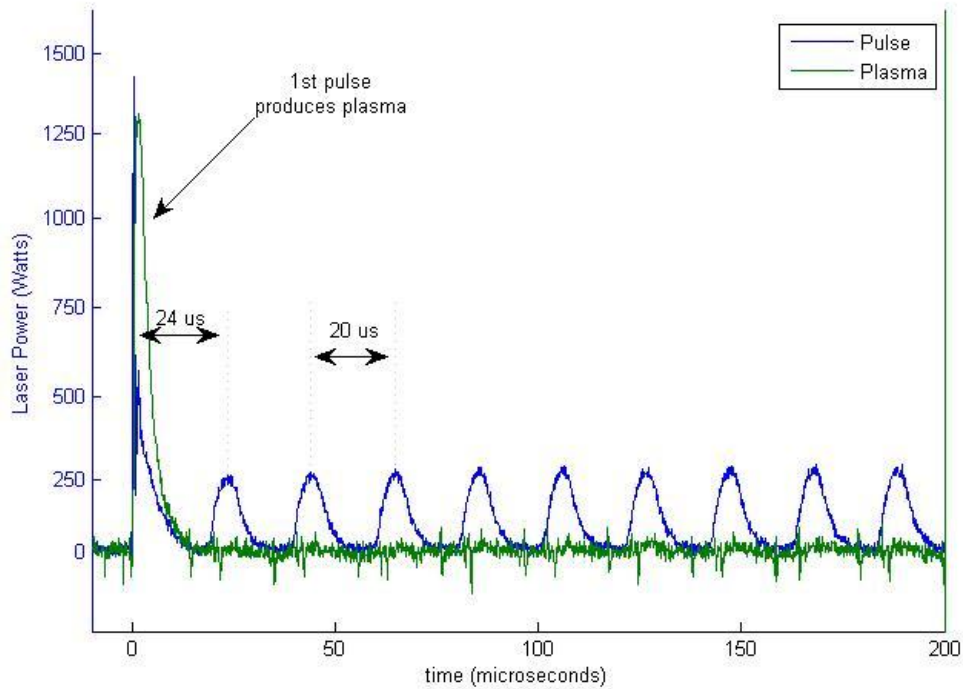


Figure 8.7-3: Pulse Waveform and Plasma Intensities of 10 Pulses at 48.7 kHz

Finally, the maximum pulsing frequency of 48.7 kHz is tested. Frequencies higher than 48.7 kHz result in steady state output rather than individual pulses. At the maximum frequency the initial spike maintains its integrity while subsequent pulses reach the steady state operating rating of the laser. Plasma intensities support the trend of no plasma formation after the initial pulse.

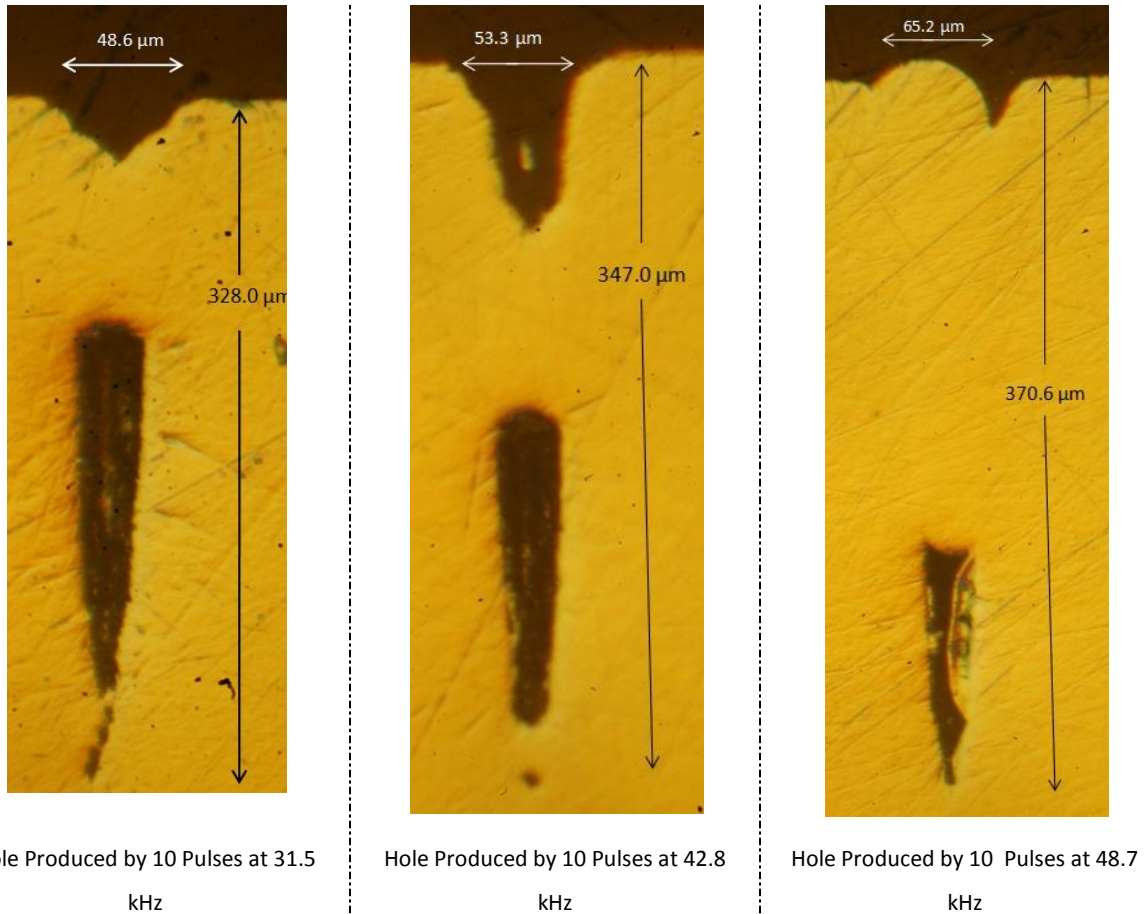


Figure 8.7-4: Hole Profiles Created at Different Pulsing Frequencies

Shown above are the results from increasing the pulsing frequency. Each increase in frequency, holding the number of pulses at 10, created an increase in depth to a maximum value of 370.6 μm . The hole width also increased to 65.2 μm . This is due to increased melting and less violent vapor/plasma ejection. As the frequency increased, a thicker layer of blocking material is formed in the hole creating unfavorable results. All holes experienced increased heat affected zones as witnessed by radial cracking along the cavity walls.

The notion of minimal plasma creation and ejection is justified by Figure 8.7-21 – 9.6-4. The lack of plasma after the initial pulse shows laser power is not sufficient to form plasma at the bottom of the cavity and that rising material does not have time to sufficiently cool for solidification. Ejection methods are again by rising vapor. The re-solidified material present most likely occurred once pulsing ceased.

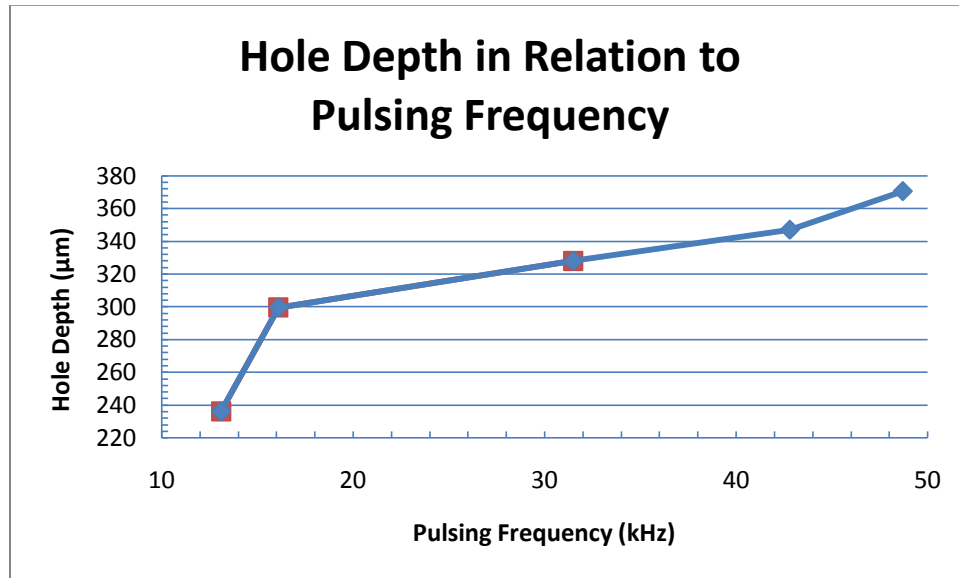


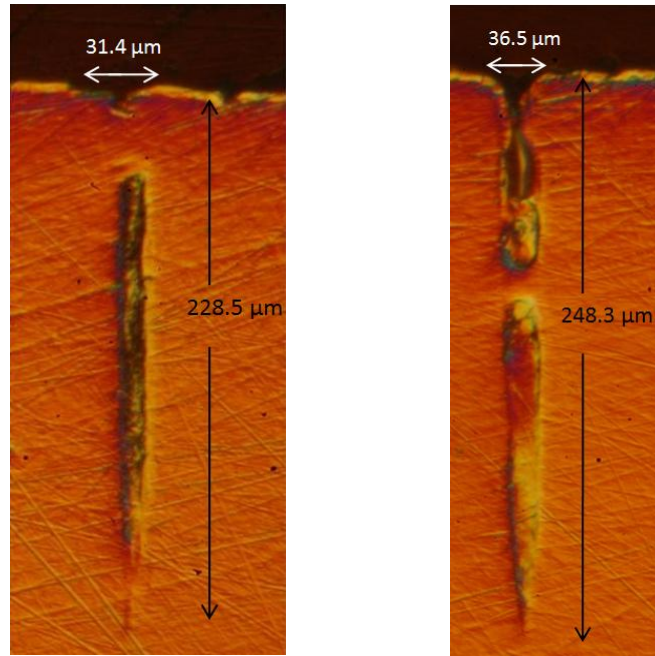
Figure 8.7-5: Hole Depth in Relation to Pulsing Frequency

Figure 8.7-5 shows frequency positively affects the depth of the hole. Physically, the secondary pulses are able to penetrate into the hot vapor quicker as frequency increases. This increases energy transfer and maintains high temperatures in the exiting vapor, increasing process efficiency. Comparing Figure 8.7-4, Figure 8.6-3, Figure 8.5-3 it can be concluded blockage increases with frequency. This is paralleled also to increased depth. The laser energy is not sufficient to expel all exiting vapor before it solidifies. Also, there appears to be an optimal frequency at which the deepest clean blind hole will be produced.

8.8 Group Multiple Pulse Drilling

Determination of the ideal pulsing length and frequency have let to improvements in hole depth. At the deepest, extreme hole blockage occurred; creating a non-usable cavity.

Techniques in group pulsing were investigated and the results follow.



Hole Profile of 2nd Single Pulse

Hole Profile of 3rd Single Pulse

Figure 8.8-1: Hole Profiles from Group Single Pulse Drilling

As expected, the introduction of extra energy, by means of more pulses, increased the holes depth and diameter. The increased depth also created the complication of material ejection as it must travel a longer distance from the bottom of the cavity to the exit hole. This extra length allows the vapor to solidify near the top of the hole after the second pulse.

Introduction of the third pulse frees the hole, deepens the hole, and vaporizes more material.

Again, the exiting energy is not enough to overcome the distance and the escaping vapor is trapped within the cavity.

Interesting of note is the efficiency of three individual pulses compared to three high frequency pulses. Comparing the depth of a single high spike followed by 2 spikes of lower power, Figure 8.3-4, with the depth of group pulsing consisting of 3 pulses, it is apparent the efficiency increases. With depths nearly equal, 248 μm and 236 μm , efficiency is greatly increased by inputting energy into still hot melt and vapor. Power densities for the group pulsing are extremely high for all three pulses while repetitive pulsing lacks power densities for the second and third pulses. Still able to reach comparable depth shows the energy is more efficiently absorbed into the material.

Still, the hole depth is not that experienced by ten pulses at 48.7 kHz. Investigation into group pulsing of ten pulses at 48.7 kHz are shown below.

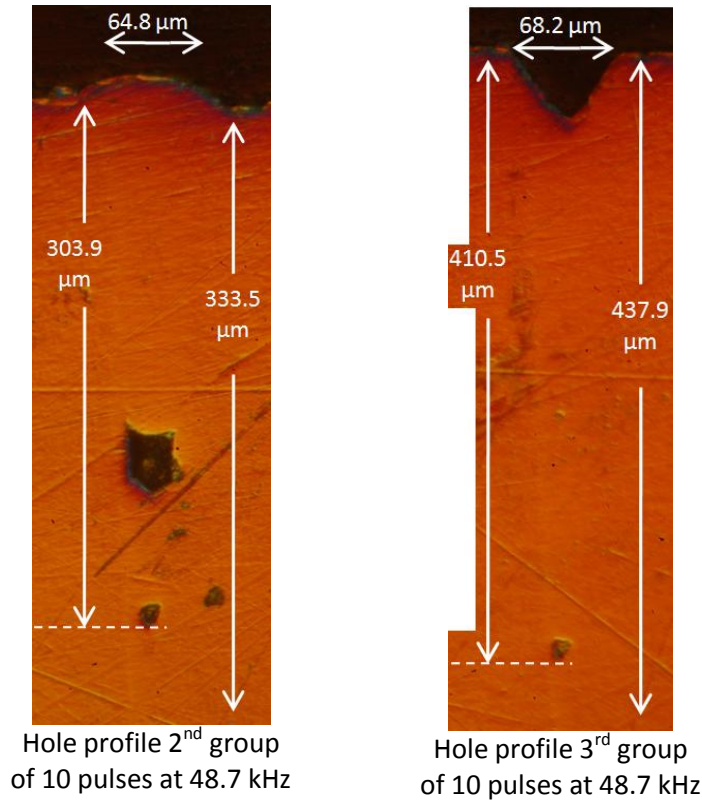


Figure 8.8-2: Hole Profiles from Group 10 Pulse Drilling

As with the group single pulse results, hole depth and width increase. Group multiple pulse does not alleviate the issue of blockage as witnessed by Figure 8.8-2. While small voids do exist, holes are mainly filled with molten material. The low pulse energy creates significant thermal affects and melt within the cavity. This melt solidifies within the cavity blocking it completely. A close look reveals the outline of the holes as the material properties change at the hole/material boundary.

8.9 Through Drilling

In order to more clearly investigate the effects of frequency, through holes were drilled in both 800 micron and 1.1 mm samples at rates of 13 kHz and 20 kHz. An InGaAs photodiode was placed below the surface of the sample, thus capturing laser light only after a through hole is formed. This allowed for the determination of time for penetration and the calculation for the number of pulses required.

A sample of 800 microns thick required times of .634 seconds and 0.0219 seconds at 13 kHz and 20 kHz, respectively, to drill through. Figure 8.9-1 and Figure 8.9-2, depict the readings from the photodiode below the sample.

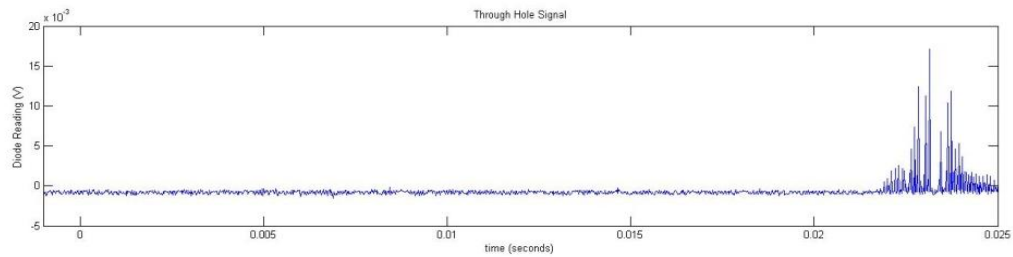


Figure 8.9-1: Time required for a through hole of 800 microns at 20 kHz

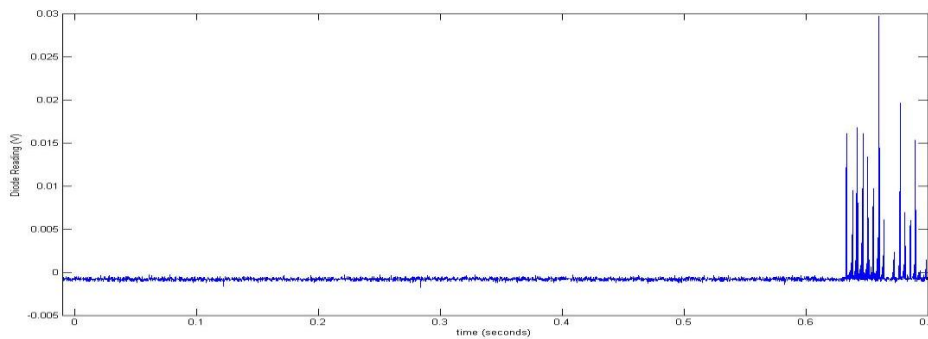
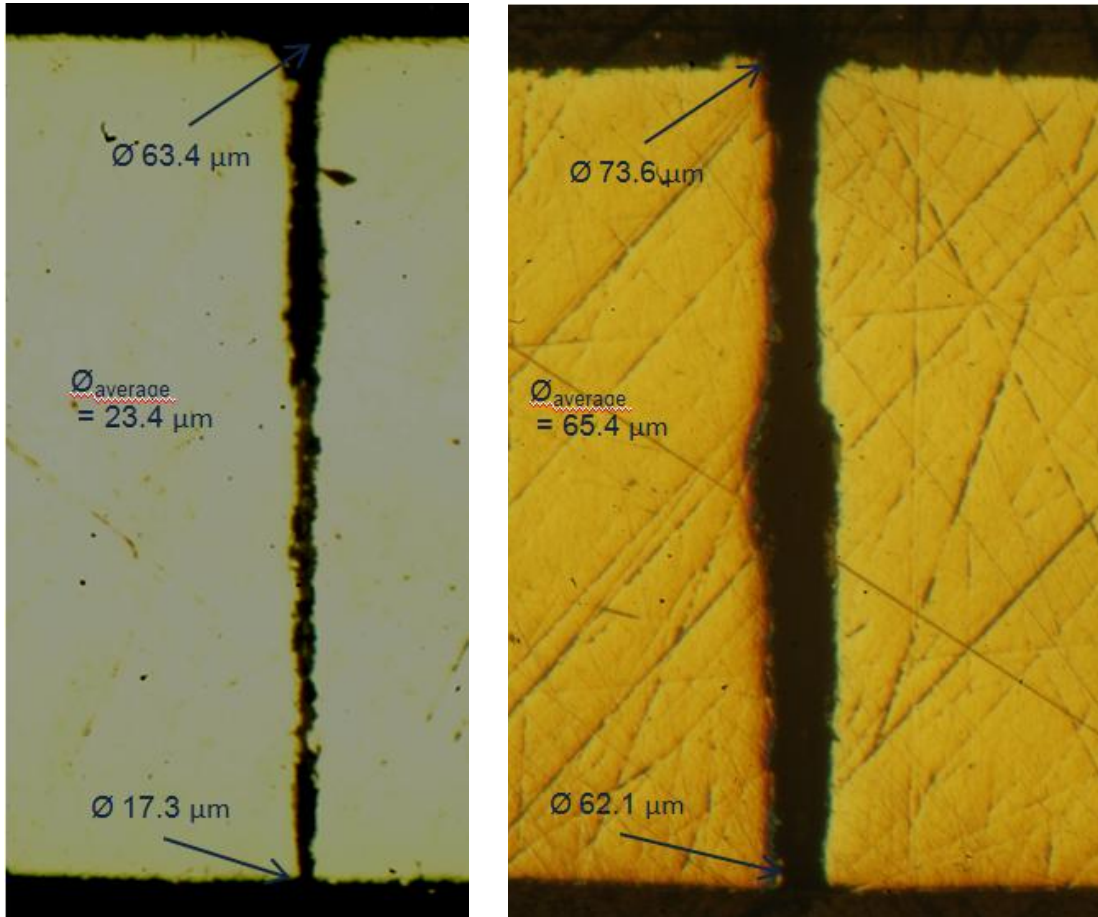


Figure 8.9-2: Time required for a through hole of 800 microns at 13 kHz

For the same sample thickness the 20 kHz regime required a mere 438 pulses while 13 kHz required 8240 pulses. Knowing the energy per pulse is consistent, a drastic reduction of pulses required is proof of better energy/material coupling with increased frequency.



Hole Profile of 800 micron hole at 13 kHz

Hole Profile of 800 micron hole at 20 kHz

Figure 8.9-3: Hole Profiles of 800 Micrometer Through Holes

Figure 8.9-3 shows the effects of pulsing frequency on hole profiles. As shown, the slower repetition rate created a narrower hole with smaller entrance and exit diameters. This can be attributed to the consistently higher process temperatures in the 20 kHz pulsing experiment.

Higher temperatures created more melt, and thus a wider hole throughout the sample. Lower frequency created higher aspect ratio hole at the cost of much longer pulse time requirements.

1.1 millimeter through hole results echoed findings at 800 microns. Below are the figures depicting the photodiode readings for through hole formation.

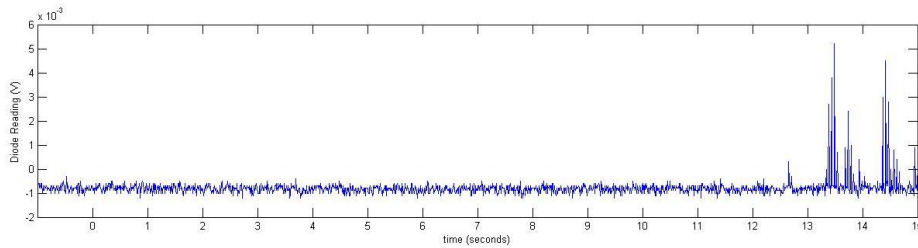


Figure 8.9-4: Time required for a through hole of 1.1 mm at 13 kHz

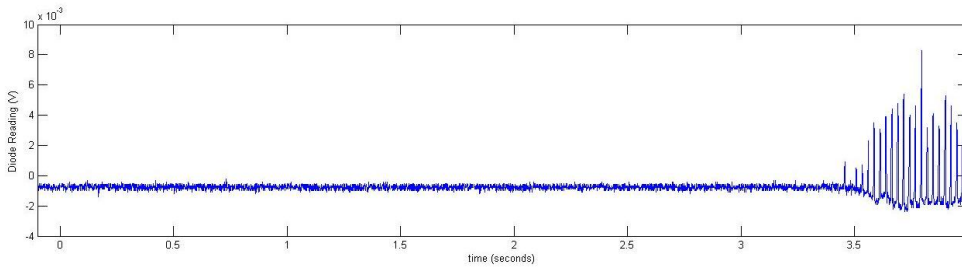
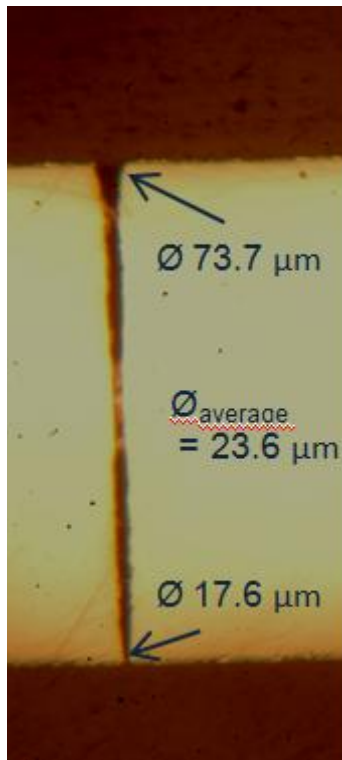


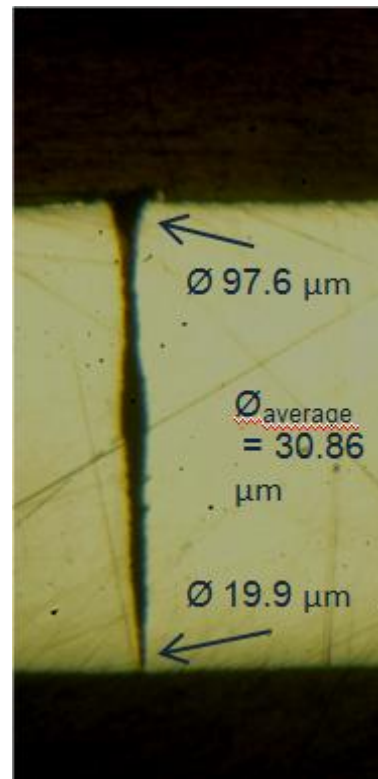
Figure 8.9-5: Time required for a through hole of 1.1 mm at 20 kHz

Once again, a drastic reduction is seen when switching to 20 kHz. Improvements in energy absorption reduced the number of pulses from ~175,000 pulses to ~70,000. The process efficiency increased 2.5 times with higher repetition of pulses. This again supports the notion

of higher repetition rates maintaining high temperatures within the holes creating better energy coupling.



Hole Profile of 1.1 mm hole at 13 kHz



Hole Profile of 1.1 mm hole at 20 kHz

Figure 8.9-6: Hole Profiles of 800 Micrometer Through Holes

The above figure depicts both 1.1 mm holes created. As with previous findings, the slower repetition rate created holes with smaller entrance and exit diameters as well as smaller average widths. The 20 kHz hole experienced inconsistencies in hole width. High temperatures caused high amounts of melt within the hole which led to trapped melt and vapor. This affected the surrounding material creating uneven hole diameters.

9 Summary

The effect of four variables on micro-hole drilling in the microsecond laser ablation regime were investigated. Changes in the pulse length, effects of high initial power densities, effects of increased frequency, and the effectiveness of group pulsing were correlated to hole depth and aspect ratio of holes on steel.

The first investigation, that of pulse length, revealed the highest aspect ratio hole by a single pulse occurs at an energy input of $\sim 3 \mu\text{s}$. Hole depths were nearly $200 \mu\text{m}$ with widths $\sim 22 \mu\text{m}$. Longer pulses increased thermal damage and wider hole diameters. Pulses shorter lacked the power density to create vapor and plasma for effective material removal.

Secondly, high power densities at the onset of pulses proved ineffective in increasing hole depth. The energy inputted by both examples is nearly equal, and therefore hole depth were comparable. The high power spikes did however aid in material removal as the ability to create plasma at high power improved material ejection.

The third variable tested was frequency. The maximum laser pulsing rate, before it emits steady state power, is 48.7 kHz . At this frequency, hole depths of $370 \mu\text{m}$ were drilled with 10 pulses. The hole width was 65 microns. Major drawbacks were the extreme blockage by solidified material. Plasma measurements illustrated the lack of power spikes limits material ejection to vapor and hot melt. The material lacking sufficient energy for exit is caught in the cavity blocking the hole. Conclusions drawn also show less blockage at lower frequency, thus an optimal frequency occurs not at the maximum frequency. Finally, an optimal blind hole depth between $240 \mu\text{m}$ and $330 \mu\text{m}$ can be created block free.

The final paradigm was that of group pulsing. The first test, pulsing one hole 3 times with a single pulse, formed holes 250 microns deep with diameters $\sim 36 \mu\text{m}$. Initially the hole was clear of blockage, consistent with initial tests. The second and third pulses, due to increased

hole depth, deepened the cavity but did not supply sufficient energy to clear the hole of blockage. Plasma was formed with each pulse but the hot vapor and melt did not escape before re-solidifying. Also, comparing the group pulsing with three single pulses to the three pulse regime earlier, it was shown process efficiency is improved by imparting the second and third pulses before material solidifies in the whole. Similar findings occurred with group pulsing of 10 pulses at 48.7 kHz. The initial pulse experienced extreme blockage. The issue was not cleared by the second or third groups of pulses. Again, the blockage was cleared and the laser energy penetrated the bottom of the cavity. Rising vapor, due to the lack of energy sufficient for vaporization, did not exit the cavity.

Through hole tests further illustrated efficiency increases with more rapid pulsing. An 800 micron through hole was successfully drilled using only 5% as many pulses for higher repetition. 1.1 mm through holes required 40% the pulses. This clearly indicates drastic efficiency benefits with higher repetition rates.

REFERENCES

1. **Ready, J. F.** *Industrial Applications of Laser*. San Diego, CA : Academic Press, 1997.
2. **Ready, John F.** *LIA Handbook of laser materials processing*. 2001.
3. **Steen, W. M.** *Laser Material Processing*. London : Springer, 1991.
4. **Dahotre, Narendra B. and Harimkar, P. Sandip.** *Laser Fabrication and Machining of Materials*. New York : Springer Science + Business Media, LLC, 2008. ISB 978-0-387-72343-3.
5. **Steen, William M.** *Laser Material Processing*. s.l. : Springer-Verlag London Limited, 1998.
6. **Bejan, Adrian and Kraus, Allan D.** *Heat Transfer Handbook*. Hoboken, New Jersey : John Wiley and Sons, 2003.
7. *Plasma shielding effect in laser ablation of metallic samples and its fluences on LIBS analysis.*
Aguilera, J. A., Aragon, C. and Penalba, F. s.l. : Appl. Surface Sciences, 1998, Vols. 127-129, pp. 309-314.
8. *Reheating of a Laser-Produced Plasma by a Second Pulse Laser.* **Uebbing, J., et al.** 9, s.l. : Applied Spectroscopy, 1991, Vol. 45, pp. 1391-1570.
9. **Elliott, David L.** *Ultraviolet Laser Technology and Applications*. San Diego, California : Academic Press, Inc., 1995.
10. **Von Allmen, M. and Blatter, A.** *Laser-Beam Interactions with Materials*. Berlin : Springer, 1995. pp. 5460-5463.
11. **Bloembergen, N.** *Laser Spectroscopy IX*. San Diego, California : Academic Press, Inc., 1989. p. vii.
12. **Brees, F. and Cross, L.** College Park, Maryland : Appl. Spectroscopy, 1962. International Conference of Spectroscopy. Vols. 16, 59.
13. **Muray, J.J.** 77, s.l. : Bull. Am. Phys. Soc, 1963, Vol. 8.
14. *A brief history of laser ablation.* **Miller, John C.** 1993. AIP Conf. Proc. Vol. 288, pp. 619-622.
15. *On the physics of short laser pulses.* **Hüttner, B.** s.l. : Lasers in Engineering, 1999, Vol. 8, pp. 319-337.

16. *Femtosecond laser-induced heating of electron gas in aluminium.* **Rethfeld, B., et al.** s.l. : Appl. Surf. Sc, 1996, Vol. 96, pp. 109-112.
17. *Fundamental aspects in machining metals with short and ultrashort laser pulses.* **Breitling, Detlef, Ruf, Andreas and Dausinger, Friedrich.** Bellingham, Wa : Proc. of SPIE, 2004, Vol. 5339, pp. 49-63.
18. *Parametric study to improve laser hole drilling process.* **Yilbas, B.S.** s.l. : Journal of Materials Processing Technology, 1997, Vol. 70, pp. 264-273.
19. **Pronko, P.P., et al.** 106, s.l. : Opt. Commun., 1995, Vol. 114.
20. **Momma, C., et al.** 134, s.l. : Opt. Commun, 1996, Vol. 129.
21. **Stuart, B.C., et al.** 459, s.l. : J. Opt. Soc. Am. B, 1996, Vol. 13, p. 459.
22. *Hole drilling in stainless steel and silicon by femtosecond pulses at low pressure.* **Juodkazis, S., et al.** s.l. : Appl. Phys. A, 2004, Vol. 79, pp. 1555-1559.
23. *Efficient submicron processing of metals with femtosecond UV pulses.* **Bekesi, J., Klein-Wiele, J. - H and Simon, P.** s.l. : Appl. Phys. A, 2003, Vol. 76, pp. 355-357.
24. *Deep drilling of metals by femtosecond laser pulses.* **Kamlage, G., et al.** s.l. : Appl. Phys. A, 2003, Vol. 77, pp. 307-310.
25. *Initiation of an early stage plasma during picosecond laser ablation of solids.* **Mao, Samuel S., et al.** s.l. : Applied Physics Letters, 2000. Vol. 11, pp. 2464-2466.
26. *Picosecond laser ablation of thin copper films.* **Jandeleit, J., et al.** s.l. : Appl. Phys. A, 1996, Vol. 63, pp. 117-121.
27. *Femtoseconds, picosecond, and nanosecond laser ablation of solids.* **Chichkov, B.N., et al.** s.l. : Appl. Phys. A, 1996, Vol. 63, pp. 109-115.
28. *Comparison of Drilling Rates and Material Removal Dynamics for Nanosecond and Femtosecond Laser Pulses.* **Semak, V. V., Thomas, J. G. and Campbell, B. R.** Bellingham, Wa : Proc. of SPIE, 2005, Vol. 5713, pp. 516-521.
29. *Femtosecond versus picosecond laser ablation.* **Ostendorf, A., et al.** Bellingham, Wa : Proc. SPIE, 2005, Vol. 5713, pp. 1-8.

30. *Influence of laser parameters and materials properties on micro drilling with femtosecond laser pulses.* **Zhu, X., et al.** s.l. : Appl. Phys.A, 1999, Vol. 69 [Suppl.], pp. S367-S371.
31. *Microsecond Laser Material Processing at 1.06 μ s.* **Garnov, S. V., et al.** 6, s.l. : Laser Physics, 2004, Vol. 14, pp. 910-915.
32. *Theoretical determination of the ablation rate of metals in multiple-nanosecond laser pulses irradiation regime.* **Stafe, Mihai, Negutu, Constantin and Popescu, Ion M.** s.l. : Elsevier B.V., 2007, Vol. 253, pp. 6353-6358.
33. *Enhanced drilling using a dual-pulse Nd:YAG laser.* **Lehane, C. and Kewok, H.S.** s.l. : Appl. Phys. A, 2001, Vol. 73, pp. 45-48.
34. *Double-pulse machining as a technique for the enhancement of material removal rates in laser machining of metals.* **Forsman, A. C., et al.** 1, s.l. : Journal of App; Phys., 2005, Vol. 98, pp. 1-6.
35. **Campbell, B. R., et al.** Performance of picosecond laser pulse drilling, including an evaluation of the double pulse machining method.
36. *On the Mechanisms of Laser-Material Interaction.* **Paleocrassas, Alexander G., et al.**
37. *Heat transfer and phase change during picosecond laser ablation of nickel.* **Willis, David A. and Xu, Xianfan.** 19, s.l. : International Journal of Heat and Mass Transfer, 2002, Vol. 45, pp. 3911-3918.
38. *Single-pulse drilling study on Au, Al, and Ti alloy.* **Cheng, J., et al.** s.l. : Appl. Phys. A, 2009, Vol. 95, pp. 739-749.
39. *Ablation of metal films by picosecond laser pulses imaged with high-speed electron microscopy.* **Bostanjoglo, I., Niedrig, R/ and Wedel, B.** 5, s.l. : J. Appl. Phys, 1994, Vol. 76, pp. 3045-3048.
40. *Microdrilling of metals with an inexpensive and compact ultra-short-pulse fiber amplified microchip lasr.* **Ancona, A., et al.** s.l. : Appl. Phys. A, 2009, Vol. 94, pp. 19-24.
41. *Double Pulse Laser Ablation and plasma: Laser Induced breakdown spectroscopy signal enhancement.* **Babushok, V. I., et al.** 9, 999-1014 : Atomic Spectroscopy, 2006, Vol. 61.
42. *Laser abltion inductively coupled plasma mass spectrometry: achievements, problems, prospects.* **Durrant, Steven F.** s.l. : Journal of Analytical Atomic Spectrometry, 1999, Vol. 14, pp. 1385-1403.
43. *Short-Pulse laser ablation of solid targets.* **Momma, Carsten, et al.** 1-2, s.l. : Optics Communcations, 1996, Vol. 129, pp. 134-142.

APPENDIX

Appendix I

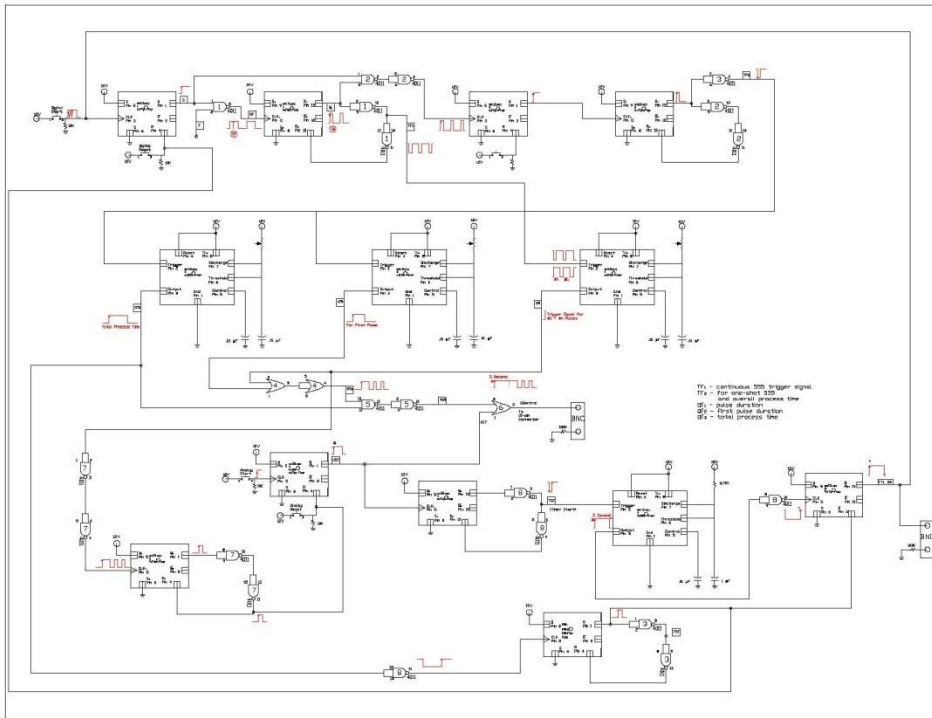


Figure 1: Combined Pulse Modulation Circuit